AN ABSTRACT OF A THESIS

PRESSURE AND VELOCITY VARIATION IN A FABRIC AIR DISPERSION SYSTEM

James Scott Leverette

Master of Science in Mechanical Engineering

An experimental program was implemented to study the pressure and velocity variations longitudinally along fabric air dispersion systems. The goal of these tests was to derive and experimentally verify a numerical model to accurately predict these values in order to aid in the design of new systems. Euler's method was used to solve the coupled energy and mass flow equations. The results of the model were compared to that of the data gathered and showed a high fidelity with only 3% error. Additional analysis was performed regarding the effects of adding extra flow resistance on the volumetric flow distribution in the system. It was determined numerically that additional flow resistance provided by an internal skeleton and/or a variable area orifice in the system does increase the uniformity of the volumetric flow pattern by at least 4%.

www.manaraa.com

المنارة للاستشارات
www.manaraa.com

PRESSURE AND VELOCITY VARIATION IN A FABRIC AIR DISPERSION SYSTEM

A Thesis

Presented to

the Faculty of the Graduate School

Tennessee Technological University

by

James Scott Leverette

In Partial Fulfillment

of the Requirements for the Degree

MASTER OF SCIENCE

Mechanical Engineering

December 2013

www.manaraa.com

UMI Number: 1548494

All rights reserved

INFORMATION TO ALL USERS
The quality of this reproduction is dependent upon the quality of the copy submitted.

In the unlikely event that the author did not send a complete manuscript
and there are missing pages, these will be noted. Also, if material had to be removed,
a note will indicate the deletion.

UMI 1548494

Published by ProQuest LLC (2013). Copyright in the Dissertation held by the Author.

Microform Edition © ProQuest LLC.
All rights reserved. This work is protected against
unauthorized copying under Title 17, United States Code

ProQuest LLC.
789 East Eisenhower Parkway
P.O. Box 1346
Ann Arbor, MI 48106 - 1346

www.manaraa.com

Copyright © James Scott Leverette 2013

All rights reserved

www.manaraa.com

CERTIFICATE OF APPROVAL OF THESIS

PRESSURE AND VELOCITY VARIATIONS IN A

FABRIC AIR DISPERSION SYSTEM

by

James Scott Leverette

Graduate Advisory Committee:

_____	_____
Stephen A Idem, Chairperson	Date
_____	_____
John Peddieson	Date
_____	_____
Glenn Cunningham	Date

Approved for the Faculty:

_____

Francis Otuonye
Associate Vice President for
Research and Graduate Studies

_____

Date

www.manaraa.com

DEDICATION

This work is dedicated to my family, friends, and mentor

www.manaraa.com

ACKNOWLEGEMENTS

I would like to thank Dr. Stephen Idem for serving as the chair of my committee and for working with me extensively through this entire process. I would also like to thank the other members of my advisory committee, Dr. Glenn Cunningham and Dr. John Peddieson.

I am very grateful for Dr. Cunningham encouraging me to stay on for graduate school and to Dr. Ken Currie and the Center for Manufacturing Research for funding my degree. I am also thankful for the support that my family provided and for the friends who helped me along the way to be where I am today.

www.manaraa.com

Table of Contents

www.manaraa.com

LIST OF TABLES

www.manaraa.com

LIST OF FIGURES

www.manaraa.com

Figure Page

www.manaraa.com

NOMENCLATURE

A	=	area, m^2 (ft^2)
A_f	=	fabric area, m^2 (ft^2)
A_0	=	orifice area, m^2 (ft^2)
D	=	duct diameter, m (ft)
f	=	friction factor, dimensionless
g	=	gravitational constant, $\frac{m}{s^2}$ $\left(\frac{ft}{s^2}\right)$
h_f	=	head loss
K_f	=	fabric coefficient, dimensionless
K_0	=	orifice coefficient, dimensionless
L	=	length of ductwork, m (ft)
L'	=	separation distance, m (ft)
$\dot{m}_x$	=	local mass flow rate, $\frac{kg}{s}$ $\left(\frac{lbm}{s}\right)$
N	=	number of elements, dimensionless
p_x	=	local gage pressure, Pa (in. wg)
Δp	=	pressure difference between duct interior and ambient, Pa (in. wg)
Q	=	volumetric flow rate, $\frac{L}{s}$ (cfm)
Q'	=	volumetric flow rate per unit area, $\frac{m}{min}$ $\left(\frac{ft}{min}\right)$
Re	=	Reynolds number, dimensionless
T	=	total pressure, Pa (in. wg)
V	=	velocity, $\frac{m}{s}$ $\left(\frac{ft}{s}\right)$
$\overline{V}$	=	average velocity, $\frac{m}{s}$ $\left(\frac{ft}{s}\right)$
V_x	=	Local velocity, $\frac{m}{s}$ $\left(\frac{ft}{s}\right)$
x_i, y_i	=	variables
ϵ	=	absolute roughness, mm (ft)
μ	=	dynamic viscosity, $\frac{N \cdot s}{m^2}$ $\left(\frac{lbm}{s\ ft}\right)$
ρ	=	density, $\frac{kg}{m^3}$ $\left(\frac{lbm}{ft^3}\right)$

www.manaraa.com

CHAPTER 1

INTRODUCTION

This thesis presents a numerical model to predict pressure and velocity variations within a fabric air dispersion system (FADS). Additional analysis was performed to determine the volumetric flow distribution along the longitudinal axis. This project was intended to provide outside testing and verification of performance claims made by a manufacturer of such systems, and will aid in their future design work. The goal of the model developed was to improve the design process of FADS by incorporating standard HVAC design techniques that use a rigorous analytical approach, instead of relying on 'rules of thumb'. Analysis was performed to determine the effect of increasing the flow resistance in the ductwork. This extra resistance is found in many systems and can be caused in several ways, including the addition of a rigid, internal skeleton or a variable area orifice. The intention of this investigation was to determine whether this added resistance improved the uniformity of the flow.

Fabric air dispersion systems are low pressure extended plenums where the duct is pressurized. Ideally the air is distributed uniformly along its path. There are three types of air dispersion styles, where (i) a porous material is used as an outlet, (ii) the fabric has linear slot outlets, and (iii) the fabric possesses circular orifices arrayed in a variety of geometric patterns along the duct length. Fabric air dispersion systems are utilized extensively in large, open ceiling facilities. Several common applications include gymnasiums, warehouses, manufacturing facilities and large retail structures. FADS are composed of textiles and possess a number of inherent advantages over metal ductwork. Textiles are significantly cheaper than metal to purchase. Significant savings in both time

www.manaraa.com

and manpower for the installation of these systems are realized due to being lightweight such that a simple hangar system can be used. Being textiles, their properties can be altered to be flame retardant or inhibit microbial growth via various treatments. There is less condensation in FADS compared to traditional systems. The aesthetic look is highly customizable due to the nature of textiles. Hence, it can be readily seen that FADS are effective and appealing. However, there is a lack of models available to aid in the prediction of performance characteristics for these systems. This project will aid in improving the design of FADS.

The research presented in Nigam et al. (2003) examined duct leakage. Traditional sheet metal duct was examined at seams and connection points. A power-law model was found to closely model the actual leakage. In Chen et al. (2010) a FADS was modeled using Fluent® and employing the standard k-ε turbulence model. It was found that the air was discharged perpendicular to the primary flow axis of the ductwork. In Chen et al. (2011) the model predictions were matched with flow visualization experiments conducted with dry ice. It was concluded that internal static pressure increases along the primary flow axis incrementally throughout the system. Some of the previous testing performed on FADS was conducted on non-permeable ductwork treated with an acrylic/urethane coating. The testing performed in Kulkarni et al. (2012) is one such case wherein the pressure losses throughout a non-porous duct were measured. They demonstrated that the internal skeleton increased the internal friction factor. It was also shown that the connection point between the fabric ductwork and the metal grid caused a variation in pressure, due to the disparity in the cross sections.

www.manaraa.com

The remainder of this thesis is organized as follows. The Chapter 2 presents the experimental program, including a description of the experimental setup and a discussion of the test procedures. Chapter 3 addresses the numerical model of fabric air dispersion system performance that was developed and verified. Therein Chapter 4 discusses the results of the tests and modeling efforts. Finally, Chapter 5 includes important observations and conclusions derived from the project, and proposes several possible subjects appropriate for further consideration.

www.manaraa.com

CHAPTER 2

EXPERIMENTAL PROGRAM

A test program was initiated to measure static pressure variation throughout a fabric air dispersion system having circular orifice outlets situated at regular intervals along the flow direction. The test procedures and data reduction strictly adhered to ANSI/ASHRAE Standard 120-2008. The air dispersion system was obtained from one manufacturer, but the design and construction was typical of fabric air dispersion systems available in North America and Europe. The nominal diameter of the test duct was 305 mm (12 in.), and in every instance the diameters of the orifices were 7.94 mm (5/16 in.). Referring to Figure 2.1, the orifices were arrayed in a triangular grid pattern along the lateral surface of the fabric duct. There were two rows of orifices on either side of the duct. The top orifice row dispersed the air parallel to the ground, while the other row was oriented at approximately 20° relative to the horizontal direction. The test duct was constructed from a porous woven fabric material. Measurements of air dispersion as a function of static pressure difference maintained across the fabric, as provided by the manufacturer, are shown in Figure 2.2. The slope of those data as calculated using a linear least squares curve-fit with the intercept forced through the origin corresponds to the fabric air diffusion coefficient. In the present instant using such an analysis, it was determined that $K_f = 262.4$ m/min·Pa (3.457 ft/min·in. wg)

The test apparatus shown in Figure 2.3 depicts the measurement locations employed in this study. The setup was in compliance with the dimensions specified in ASHRAE Standard 120. The test duct was comprised of three sections of fabric duct connected by a zipper, per the manufacturer's installation directions. Each section had a

www.manaraa.com

nominal length of 4.6 m (15 ft). One longitudinal seam was present running down the entire length of the specimen. The terminal end of the system was capped by the same fabric material. From plane 1 to plane 2, the duct had an overall length of 13.7 m (45 ft). It was suspended from the laboratory ceiling by means of a hangar system per the manufacturer's recommendations; refer to Figure 2.4. Two configurations were tested. In one instance a skeletal metal frame was inserted into the duct to maintain the duct shape in the absence of static air pressure. A schematic diagram of the internal skeleton is provided in Figure 2.5. The ring and spoke components of the frame consisted of 6.4 mm (0.25 in.) diameter steel rod, and the diameter of central aluminum spacer tube was 20.3 mm (0.8 in.). The separation distance L' between the rings was approximately 1.88 m (74 in). The skeleton system provided an adjustment means to control the distance between each ring in order to regulate the tension in the fabric duct. The rings situated at the terminal ends of the fabric duct had eight equally-spaced spokes, whereas the interior rings possessed four equally-spaced spokes. In every instance the outer diameters of the ring elements closely matched the inner diameter of the fabric duct. Additional tests were performed where the internal skeleton system was absent, and the fabric duct cross section was maintained solely by internal static pressure.

A 20 hp centrifugal fan was employed to provide air flow through the fabric air dispersion system. The flow system was blow-through in nature. A variable frequency drive (VFD) was used to control fan motor speed and regulate the flow rate through the test section. A multiple-nozzle chamber in compliance with the requirements of ASHRAE Standard 120 was used to accurately measure the volume flow rate through the test setup. Screens installed in the nozzle chamber upstream of the nozzle board were used to help

www.manaraa.com

flatten the air velocity profile entering the flow nozzles. Unused nozzles were blocked by vinyl balls. The fan motor was allowed to run for several minutes in order to obtain stable conditions. The pressure drop across the nozzles was measured using two piezometric rings located 38 mm (1.5 in.) on either side of the nozzle board. A micromanometer with a scale readability of 0.025 mm (0.001 in) was used to measure the pressure drop across the flow nozzles. A digital manometer with a scale readability of 0.25 mm (0.01 in) was employed to measure the nozzle chamber static pressure. The dry bulb temperature of the nozzle chamber was measured with a thermometer having a scale readability of 0.6°C (1°F). The ambient wet bulb and dry bulb temperatures were measured using a compact lab pyschrometer with a scale readability of 0.6°C (1°F). The atmospheric pressure was measured using a mercury barometer with a scale readability of 0.25 mm (0.01 in) of mercury.

The duct test apparatus shown in Figure 2.3 was used to measure the pressure variation throughout the fabric air dispersion system. In every instance the experimental setup consisted of a galvanized steel entrance duct section with a diameter of 305 mm (12 in.). Per ASHRAE Standard 120 the steel ducts had a length exceeding 12 duct diameters, which was sufficient to achieve fully developed flow entering the fabric duct test section. Per the installation instructions of the manufacturer the fabric duct overlapped the steel duct by a length of 229 mm (9 in.). The test duct was secured to the steel duct using a fabric strap, and the joint was further wrapped with several layers of cloth-backed duct tape with a natural latex-rubber adhesive in order to ensure an airtight connection. Pressure taps constructed from 6.4 mm (0.25 in.) diameter copper tubing were soldered onto the steel duct where it intersected the fabric duct. These pressure taps were arrayed in a piezometric

www.manaraa.com

ring. A liquid-filled micromanometer having a scale readability of 0.025 mm (0.001 in) was employed to measure the static pressure at the entrance plane of the fabric air dispersion system. The static pressure ports of Pitot-static tubes were used to measure the static gage pressure in the fabric duct. Referring to Figure 2.3, the Pitot-static tubes were mounted on stands at regular intervals of approximately 2.4 m (8 ft) along the flow axis of the fabric duct. Electronic manometers having a scale readability of 0.25 mm (0.01 in) were used to measure the local pressure in the fabric duct at each location. In every instance the Pitot-static tubes were inserted into the fabric duct through the lateral surface orifices. The Pitot-static tubes were aligned precisely with the air flow. When an internal skeleton was installed in the fabric duct, care was taken to ensure that the Pitot-static tubes were situated at least one duct diameter away from a ring, and at least 25 mm (1 in.) away from the central spacer tube. In the absence of an internal skeleton the Pitot-static tubes were located precisely at the fabric duct centerline.

In this test program the locations of the static pressure measurements, and all dimensional measurements, were assumed to have an accuracy of ±1%. In some instances, the pressure measurement uncertainty exceeded the basic scale readability of a particular instrument. Typically that occurred when random variability in the system static pressure was present, and the fluctuations exceeded the scale readability of the manometer. For the conditions encountered in the experiments, estimates of the measurement uncertainty of several quantities are presented in Table 2.1. Assuming random variations in the measured quantities, an uncertainty analysis based on the method outlined in ASHRAE Guideline 2 (2005) was performed. In every instance the measurement uncertainty estimates were performed with a 95% confidence level.

www.manaraa.com

Table 2.1. Uncertainties in Measured Parameters.

Dry-Bulb Temperature	0.6°C (1°F)
Wet-Bulb Temperature	0.6°C (1°F)
Nozzle Chamber Temperature	0.6°C (1°F)
Test Section Temperature	0.6°C (1°F)
Nozzle Chamber Static Pressure	25 Pa (0.1 in. wg)
Pressure Drop Across Nozzle Chamber	5 Pa (0.02 in. wg)
Test Section Static Pressure	2.5 Pa (0.01 in. wg)
Barometric Pressure	0.25 mm Hg (0.01 in. Hg)

www.manaraa.com

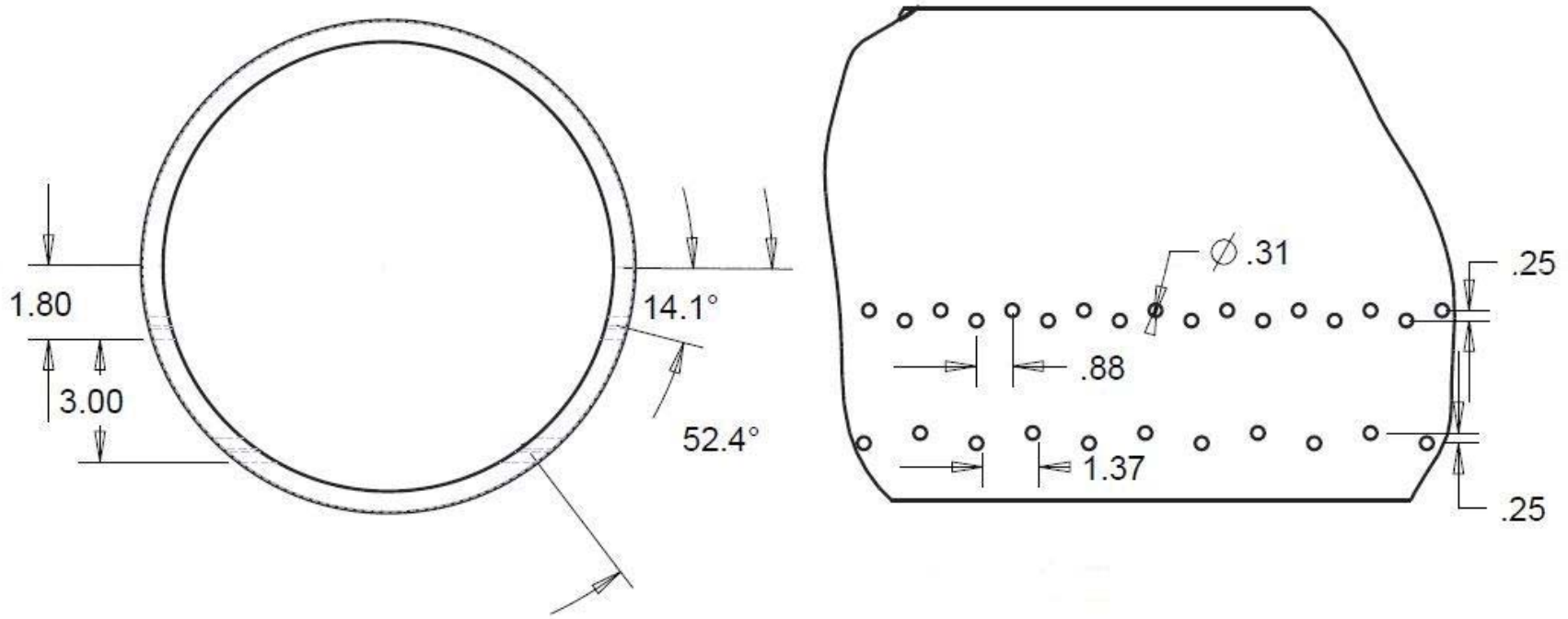

Figure 2.1. Fabric Air Dispersion System Orifice Geometry (All Dimensions Are Inches).

www.manaraa.com

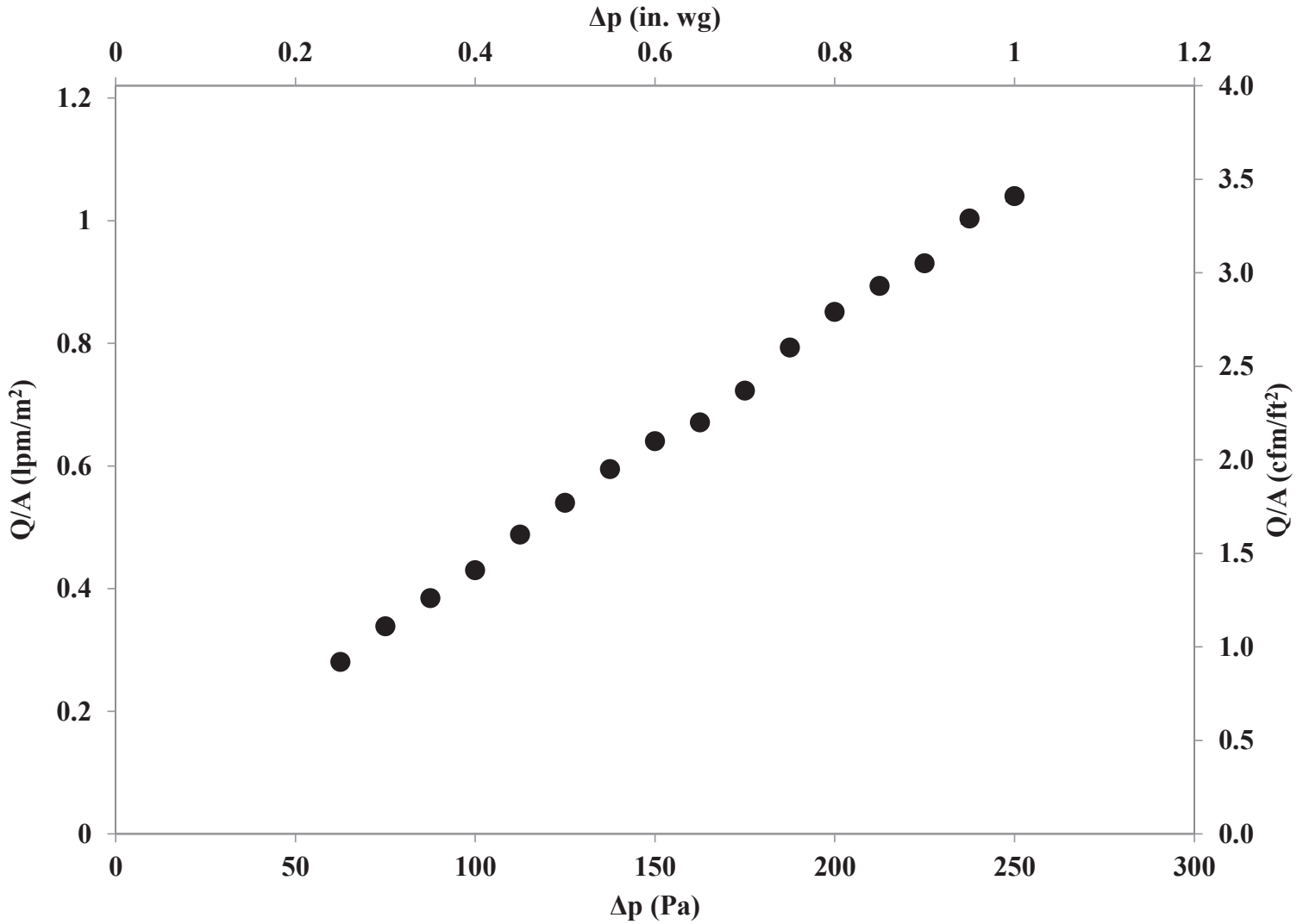

www.manaraa.com

Figure 2.2. Volumetric Flow Rate per Unit Area vs. Pressure.

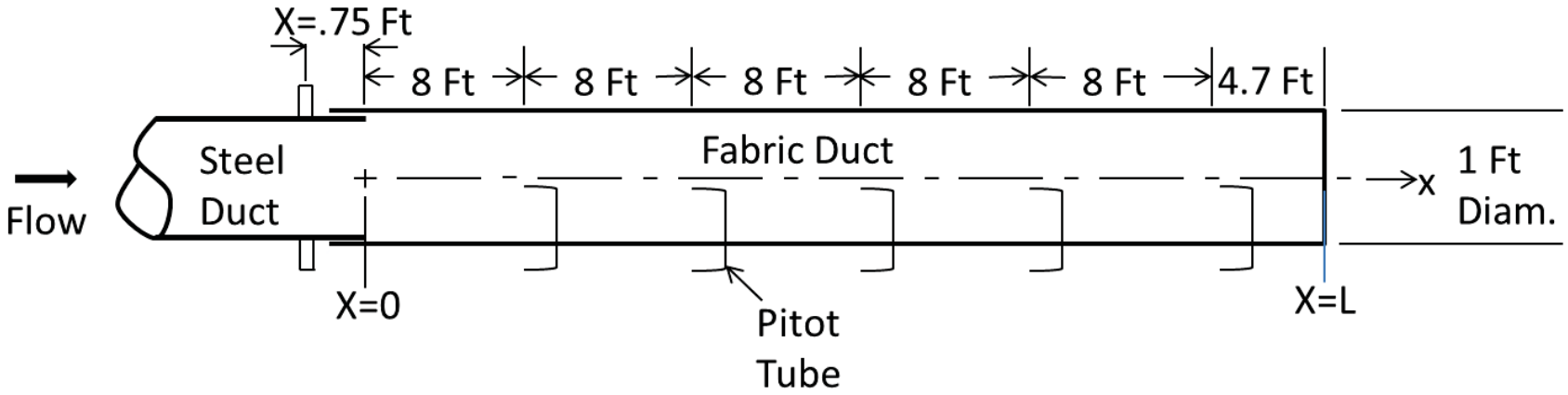

Figure 2.3. Pressure Measurement Locations (All Dimensions Are Feet).

www.manaraa.com

Figure 2.4. Hanger System.

www.manaraa.com

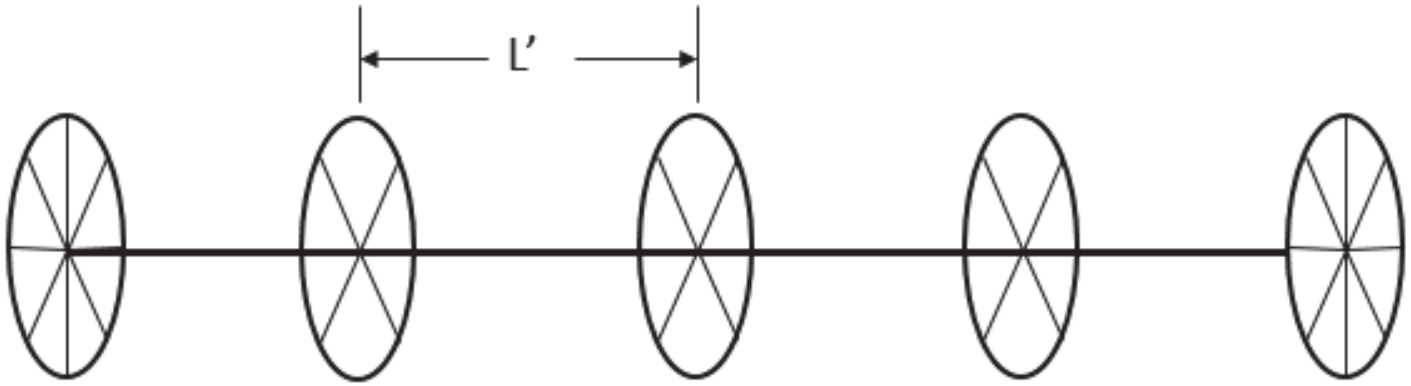

Figure 2.5. Internal Skeleton.

www.manaraa.com

CHAPTER 3

NUMERICAL MODEL

A numerical model was developed to predict the continuous static pressure and velocity variation throughout a fabric air dispersion system having circular orifices situated at regular intervals along the flow direction. The approach taken was to discretize the fabric duct into finite intervals and calculate the average pressure and air flow distribution over each increment. As outlined herein, this was achieved by conducting energy and mass balances on a representative differential control volume, and solving the resulting coupled differential equations using straightforward numerical methods.

Consider steady, incompressible, one-dimensional flow through a fabric air dispersion system. Referring to the control volume depicted in Figure 3.1, conservation of mechanical energy for a differential section of the duct can be expressed as follows

$$\frac{p_x}{\rho g} - \frac{p_{x+\Delta x}}{\rho g} + \frac{V_x^2}{2g} - \frac{V_{x+\Delta x}^2}{2g} = h_f \qquad (3.1).$$

The terms on the left hand side of this equation represent the net flow work and kinetic energy per unit weight of flowing air, respectively. The right hand side is the head loss, which is expressed in terms of the empirical Darcy friction factor. Rearranging and dividing through by Δx yields the following

$$-\frac{1}{\rho g}\frac{p_{x+\Delta x} - p_x}{\Delta x} - \frac{1}{2g}\frac{V_{x+\Delta x}^2 - V_x^2}{\Delta x} = \frac{h_f}{\Delta x} = \frac{f}{\Delta x}\frac{\Delta x}{D}\frac{\overline{V}^2}{2g} \qquad (3.2).$$

In this instance the quantity $\overline{V}$ represents the average air velocity in the differential element. This equation can be further simplified by factoring common terms. Hence in the limit as $\Delta x \rightarrow 0$, and by the definition of the derivative, the energy balance can be written in differential form

www.manaraa.com

$$-\frac{1}{\rho g}\frac{dp}{dx}-\frac{1}{2g}\frac{dV^2}{dx}=\frac{f}{D}\frac{\overline{V}^2}{2g} \tag{3.3}$$

This can be further simplified algebraically, such that

$$\frac{dp}{dx}+\rho V\frac{dV}{dx}=-\frac{f\rho}{2D}\overline{V}^2 \tag{3.4}$$

The total pressure at any location in the duct is given by

$$T=p+\frac{1}{2}\rho V^2 \tag{3.5}$$

Taking the derivative of that equation with respect to the axial coordinate x, it is straightforward to show that

$$\frac{dT}{dx}=\frac{dp}{dx}+\rho V\frac{dV}{dx} \tag{3.6}$$

This differential equation describes the change of total pressure through the duct associated with variations in the static pressure and velocity in the flow direction. Comparing Equations 3.4 and 3.6, it is apparent that the variation of the total pressure along the duct axis is given by the following 1st order differential equation

$$\frac{dT}{dx}=-\frac{\rho}{2D}f\overline{V}^2 \tag{3.7}$$

The friction factor f and the local average velocity in the duct $\overline{V}$ are functions of x along the duct. To a close approximation $\overline{V}$ can be modeled using the value air velocity entering each discrete duct segment. In that case the friction factor can also be calculated based upon the entering air velocity.

Referring to the control volume shown in Figure 3.2, conservation of mass for a differential section of the duct can be expressed in terms of the local volume flow rate per unit surface area Q' as follows

$$(\dot{m}_x-\dot{m}_{x+\Delta x})=\rho\pi D\Delta x Q' \tag{3.8}$$

www.manaraa.com

Physically this equation represents the change in mass flow through the discrete control volume due to dispersion of air through the orifices and the permeable fabric. Expressing the mass flow using the continuity equation yields

$$-\rho A(V_{x+\Delta x} - V_x) = \rho \pi D \Delta x Q' \tag{3.9}.$$

This equation can be further simplified by dividing both sides by Δx , where the duct cross section is given by $A = \frac{\pi D^2}{4}$, and canceling common terms. Hence in the limit as $\Delta x \to 0$, and by the definition of the derivative, the mass balance can be written in differential form

$$\frac{dV}{dx} = -\frac{4Q'}{D} \tag{3.10}.$$

The total volume flow rate of air from the fabric air dispersion system is the sum of the flow rates through the orifices and the fabric

$$Q = Q_0 + Q_f = \sum K_0 A_0 \sqrt{\frac{2\Delta p}{\rho}} + A_f K_f \Delta p \tag{3.11}.$$

Implicit in this expression is the assumption that the orifice coefficients K_o and the local static pressure difference between the duct interior and the environment Δp are constant over each discrete duct segment. In that case dividing through by the total surface area, the local volume flow rate per unit surface area is approximated as

$$Q' = K_0 \left(\frac{A_0}{A}\right) \sqrt{\frac{2}{\rho}} (\Delta p)^{0.5} + K_f \left(\frac{A_f}{A}\right) (\Delta p) \tag{3.12}.$$

An important implication of this expression is that Q' is a function of $(\Delta p)^n$, where $0.5 \le n \le 1.0$. Hence for a fabric air dispersion system constructed from a porous material and having circular orifices situated at regular intervals along the lateral surface of the duct, the local volume flow rate per unit surface area Q' is a weighted average of Δp raised to

www.manaraa.com

the powers of 0.5 and 1.0, respectively. Substituting (3.12) into (3.10), the variation of air velocity along the duct axis is given by the following 1st order differential equation

$$\frac{dV}{dx} = \frac{-4Q'}{D}$$

$$= \frac{4}{d}K_0\left(\frac{A_0}{A}\right)\sqrt{\frac{2}{\rho}}\left(T - \frac{1}{2}\rho V^2\right)^{.5} - \frac{4}{D}K_f\left(\frac{A_f}{A}\right)\left(T - \frac{1}{2}\rho V^2\right) \quad (3.13).$$

It is convenient to non-dimensionalize Equations 3.7 and 3.13, which respectively describe the axial variation of total pressure and velocity in a fabric air dispersion system. This is accomplished using the total pressure and velocity at the duct entrance, and the total duct length 'L'. In that case the dimensionless total pressure is defined as

$$T' = \frac{T}{\frac{1}{2}\rho {V_{ref}}^2} \quad (3.14).$$

Likewise the dimensionless velocity is given by

$$V' = \frac{V}{V_{ref}} \quad (3.15).$$

Similarly the dimensionless distance is defined such that

$$x' = \frac{x}{L} \quad (3.16).$$

Substituting the dimensionless variables defined by (3.14) through (3.16) into Equation 3.7 yields the following

$$\frac{dT\prime\frac{1}{2}\rho V_{ref}^2}{dx\prime L} = -K_1 f V_{ref}^2 = \left(\frac{\rho}{2D}\right) f V' V_{ref}^2 \quad (3.17).$$

Therein factoring common terms, it can readily be demonstrated that the total pressure variation along the duct axis is expressed as

$$\frac{dT\prime}{dx\prime} = -k_1 V'^2;\ k_1 = \frac{fL}{D} \quad (3.18).$$

Likewise substituting the dimensionless variables defined by (3.14) through (3.16) into Equation (3.13) produces the following

www.manaraa.com

$$\frac{dV'V_{ref}}{dx'L} = -\frac{4}{D}K_0\left(\frac{A_0}{A}\right)\sqrt{\frac{2}{\rho}}\left(\frac{1}{2}\rho V_{ref}^2 T' - \frac{1}{2}\rho V_{ref}^2 V'^2\right)^{.5}$$

$$-\frac{4}{D}K_f\left(\frac{A_f}{A}\right)\left(\frac{1}{2}\rho V_{ref}^2 T' - \frac{1}{2}\rho V_{ref}^2 V'^2\right) \qquad (3.19).$$

It is possible to cancel common terms, such that the air velocity variation along the duct axis is given by

$$\frac{dV'}{dx'} = -\left(\frac{4K_0 L}{D}\right)\left(\frac{A_0}{A}\right)(T' - V')^{.5} - \left(\frac{2K_f L\rho V_{ref}}{D}\right)\left(\frac{A_f}{A}\right)(T' - V'^2) \qquad (3.20).$$

In order to solve coupled differential equations (3.18) and (3.20) it is necessary to define appropriate boundary conditions. The reference velocity is a function of the known volume flow rate that must be dispersed through the system, therefore it is calculated as follows

$$V_{ref} = \frac{Q}{A} = \frac{4Q}{\pi D^2} \qquad (3.21).$$

At the duct inlet where $x = 0$ the air velocity is given by $V = V_{ref}$. Hence the boundary condition at the duct entrance is given by

$$x' = 0,\ V' = 1 \qquad (3.22).$$

The total pressure at $x = 0$ is not known a priori, and therefore it must be calculated iteratively subject to the condition that the air velocity at x = L is zero, since the terminal end of the duct is capped and it is assumed that the diffusion velocity through the fabric is negligible. In that case the remaining boundary condition is expressed as follows

$$x' = 1, V' = 0 \qquad (3.23)$$

In this study the differential equations which govern the distribution of velocity and static pressure in the fabric air distribution system, i.e., Equations 3.18 and 3.20, were solved numerically using Euler's method as described herein. Consider the general first-order initial value problem, expressed as follows

www.manaraa.com

$$\frac{dy}{dx} = F(y, x) \tag{3.23}$$

and: $$y(0) = y_0 \tag{3.24}.$$

One straightforward approach to obtaining a numerical solution to the problem is to replace dy/dx by a simple forward finite difference representation. Hence

$$\frac{y_{i+1} - y_i}{\Delta x} = F(y_i, x_i) \tag{3.25}.$$

Solving for y_{i+1} yields

$$y_{i+1} = y_i + \Delta x \cdot F(y_i, x_i) \tag{3.26}.$$

Given the initial condition described by Equation 3.24 it is possible to march forward in x from x = 0, using Equation 3.26 to obtain a value of y at each new value of x.

The previous approach can readily be extended to yield a system of first-order differential equations. Consider the following system of two equations

$$\frac{dY_{1,i+1}}{dx} = Y_{1,i} + \Delta x \cdot F_1\left(Y_{1,i}, Y_{2,i}, x_i\right) \tag{3.27}$$

and: $$\frac{dY_{2,i+1}}{dx} = Y_{2,i} + \Delta x \cdot F_2\left(Y_{1,i}, Y_{2,i}, x_i\right) \tag{3.28}.$$

Hence the numerical solution is obtained by proceeding in the direction of increasing x, starting from the initial conditions at x = 0, and successively calculating the dependent variables Y_1 and Y_2 at each step. For Euler's method the truncation error per unit step is $\sigma(\Delta x^2)$, hence small step sizes are required for numerical accuracy. In this study the method was chosen primarily because of the ease with which it can be programmed in spreadsheet applications, and other more accurate numerical integration techniques could have been employed.

Numerical integration of Equation 3.18 by Euler's method required the evaluation of the Darcy friction factor 'f', in order to determine the dimensionless parameter k_1.

www.manaraa.com

Referring to any standard fluid mechanics text, e.g., Munson et al. (2009), the friction factor depends on the Reynolds number 'Re' and the relative roughness 'ε/D'. Because the air velocity 'V' varies continuously along the flow axis of the duct in an air dispersion system, the friction factor is a local variable. In this study, the local Reynolds number was calculated as follows

$$\mathrm{Re} = \frac{\rho \mathrm{V} \mathrm{D}}{\mu} \tag{3.29}.$$

Referring again to Munson et al. (2009), the Colebrook equation is often employed to calculate the friction factor. However, since it is an implicit function of the friction factor the Colebrook equation is inconvenient for incorporation into simple design programs, because it requires an iterative solution approach. Hence in order to facilitate the numerical integration of the governing equations, an explicit formula provided in Haaland (1983) was used in the present study to evaluate the local friction factor in the air dispersion system. Therein

$$\mathrm{f} = \frac{1}{\left\{1.8 \log\left[\frac{1}{\frac{6.9}{\mathrm{Re}} + \left(\frac{\varepsilon/\mathrm{D}}{3.7}\right)^{1.11}}\right]\right\}^2} \tag{3.30}.$$

Per Kulkarni et al. (2012), in the absence of in internal skeleton to maintain the duct shape when there is no static air pressure, an absolute roughness value ε = 0.09 mm (0.0003 ft) was assumed. Similarly, in those instances where an internal skeleton was present, an absolute roughness of ε = 1.83 mm (0.006 ft) was employed in the numerical model. The air viscosity in the air dispersion system was assumed to be constant along the flow axis of the duct, and was calculated based on the ambient air temperature. In this study the viscosity required by Equation 3.29 was calculated using Sutherland's equation (White, 2006)

www.manaraa.com

$$\mu = \mu_0 \left(\frac{T}{T_0}\right)^{1.5} \left(\frac{T_0+111}{T+111}\right) \quad (3.31 \text{ SI})$$

$$\mu = \mu_0 \left(\frac{T}{T_0}\right)^{1.5} \left(\frac{T_0+198.72}{T+198.72}\right) \quad (3.32 \text{ IP}).$$

Likewise the air density in Equation 3.29 was evaluated by means of the ideal gas law

$$\rho = \frac{p}{RT} \quad (3.33).$$

The air density was assumed to be constant, and was determined using the measured ambient pressure.

The fabric diffusion coefficient K_f was available from pressure drop and flow rate data supplied by the manufacturer. However, the specific variation of the orifice coefficient in the air dispersion system was not known beforehand, and could not readily be predicted from theory. A search of the literature did not yield any empirical models for the orifice coefficient when flow occurs in the axial direction of the duct, but the flow issues in a primarily radial direction through each orifice. Ultimately it was determined by a trial and error procedure that assumption of a constant orifice coefficient $K_o = 0.50$ for all orifice locations yielded sufficiently accurate model predictions.

www.manaraa.com

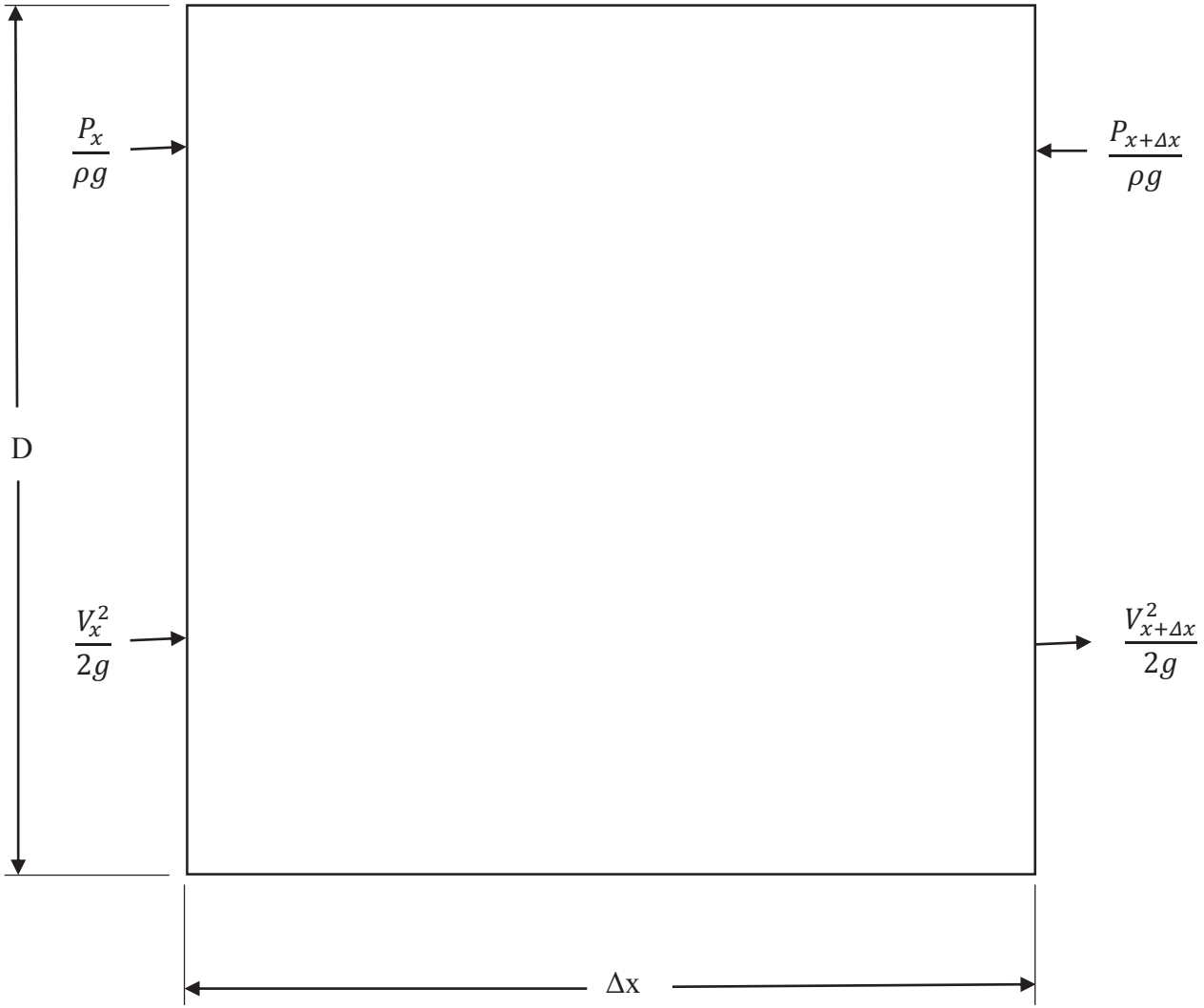

Figure 3.1. Differential Control Volume.

www.manaraa.com

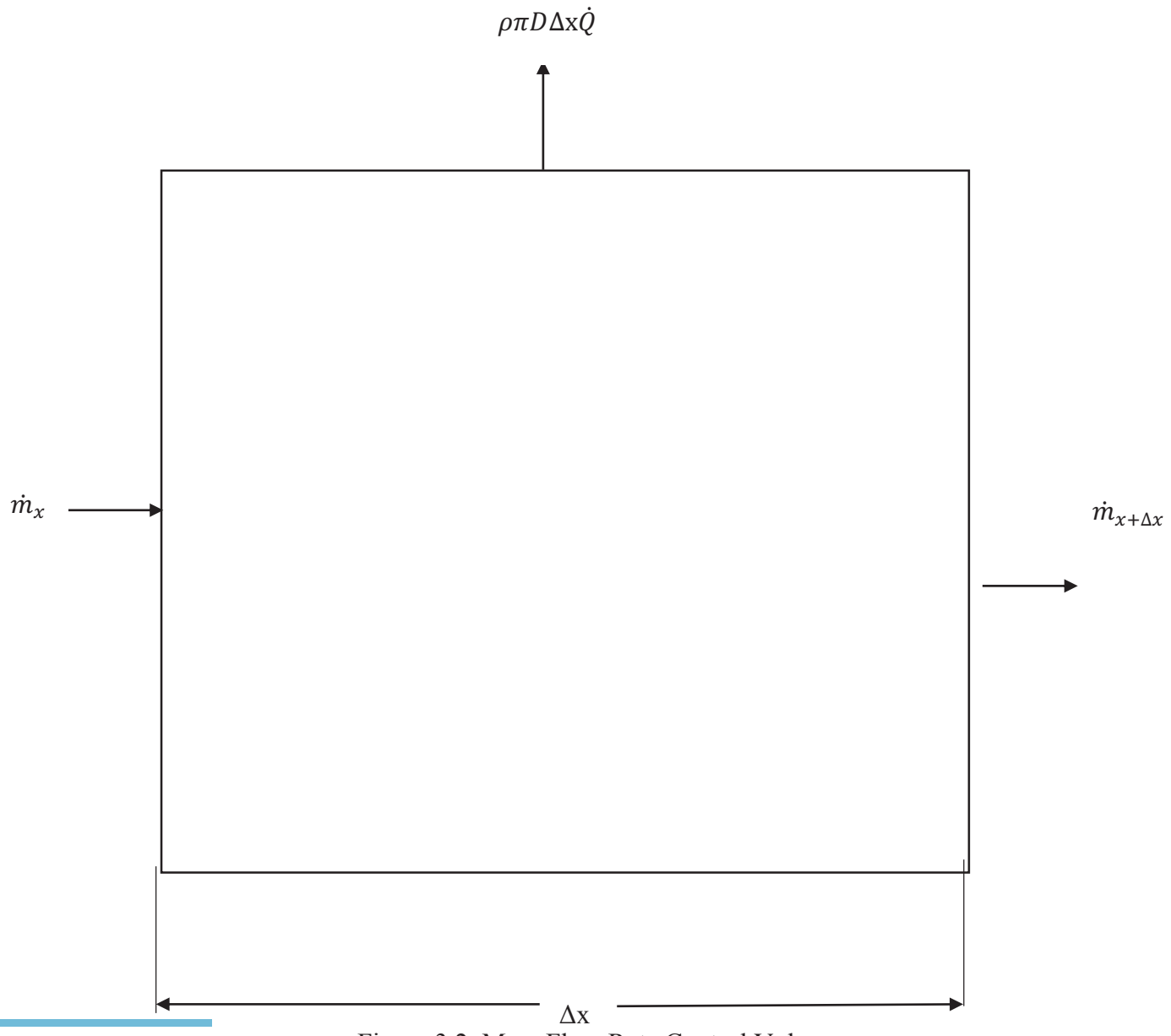

Figure 3.2. Mass Flow Rate Control Volume.

www.manaraa.com

CHAPTER 4

RESULTS

For the fabric air dispersion system described in Chapter 2, dimensional information such as the duct diameter and length, the quantity and diameters of the lateral surface orifices, as well as the relative roughness, were necessary input for the numerical performance model. In addition the model required values for the fabric diffusion coefficient and the orifice coefficient. Likewise, the model needed information related to the volume flow rate entering the system, as well as data related to ambient air density and pressure. Model verification consisted of comparing predictions of static gage pressure to measurements of the local pressure in the fabric air dispersion system, with and without an internal skeleton present. For those cases the model employed N = 80 nodes over the region $0 \leq x' \leq 1$, such that grid dimensions corresponded to $\Delta x' = 0.0125$. It was determined that halving the grid size had no discernible effect on the calculated static pressures, such that the results were deemed to be 'grid independent'. In every instance the dimensionless total pressure at the system inlet $T'(0)$ was calculated iteratively, in order to achieve an air velocity $V'(1) = 0$ at the terminal end of the duct.

Tables 4.1 and 4.2 summarize the measured static pressures as the volume flow rate entering the duct was systematically increased, for those instances where an internal skeleton was either absent or present, respectively. Therein Figures 4.1 through 4.7 compare measured static gage pressures in the fabric air dispersion system to those values predicted by the numerical model for those tests where an internal skeleton was absent from the apparatus. Similarly Figures 4.8 through 4.14 contrast measured static gage pressures to calculated values for those tests where an internal skeleton was inserted into

www.manaraa.com

the air dispersion system. For these circumstances the dimensionless total pressures at the system inlet determined by the numerical model are summarized in Table 4.3. The horizontal error bars in Figures 4.1 through 4.14 represent a dimensional measurement uncertainty of $\pm 1\%$, which was assumed throughout this study. Likewise the vertical error bars in Figures 4.1 through 4.14 depict an assumed pressure measurement error of ± 5 kPa (0.02 in. wg); that exceeds the scale readability of the electronic manometers employed in the measurements because of random pressure fluctuations which were observed during the test program. These cases correspond to instances where the Reynolds number at the duct inlet ranged from 1.20×10^5 to 3.20×10^5.

It is apparent that predictions of static gage pressure in the fabric air dispersion system generated by the numerical model described in Chapter 3 closely matched measured values, when an internal skeleton was either present or absent. The maximum deviation between measured and predicted static gage pressures for all cases was 3%, as determined by means of root mean squared analysis. That quantity was calculated as follows

$$\%\text{Error} = \sqrt{\frac{\sum[(\Delta p_{measured} - \Delta p_{calc})^2]}{N}} \times 100 \qquad (4.1)$$

In general it was observed that at any given inlet Reynolds number, the static gage pressure in the air dispersion system duct rose monotonically in the flow direction, and asymptotically approached a constant value toward the terminal end. For comparable cases of inlet Reynolds number, both measured and predicted inlet dimensionless total pressures were higher when an internal skeleton was present versus those instances where a skeleton was not employed. The presence of the skeleton imposed a penalty on the system pressure loss in the flow direction, which in turn must be compensated for by means of a higher static pressure at the duct inlet.

www.manaraa.com

A further study was conducted to characterize the uniformity of air dispersion along the flow axis of the duct described previously in Chapter 2, where the entering volume flow rate was systematically varied over a representative range. Therein identical dimensional data, e.g., duct diameter and length the quantity and diameters of the lateral surface orifices, and the relative roughness, were employed as input to the model. Likewise the analysis assumed K_o = 0.50 and K_f = 262.4 m/min·Pa (3.457 ft/min·in. wg), as well as the same ambient air density and pressure data as was used in the previous verification study. Several cases were considered, e.g., a skeleton was either absent or present in the duct. In addition, the study also investigated the situation where an adjustable flow device (a fabric orifice with an adjustable hemmed drawstring aperture) designed to locally reduce pressure was installed at the mid-point of the duct. In practice this can be achieved by means of a commercially available product that can be zipped into the fabric duct between the sections. For those cases, the presence of an internal skeleton was presumed. Such calculations were initially performed by employing the boundary condition at the duct terminal end $V'(1) = 0$, assuming a full-length duct. This yielded a value of the mid-point dimensionless velocity $V'(0.5)$, which in turn was used to calculate the volume flow rate entering a downstream half-length duct. Thereafter the calculations proceeded as before, where the dimensionless velocity at the terminal end of the half-length system was again forced to zero. For all cases considered in the study of uniform air dispersion the numerical model once again employed N = 80 nodes over the region $0 \leq x' \leq 1$.

Investigation of air dispersion uniformity for each of the cases described previously proceeded as follows. Upon solution of coupled Equations 3.18 and 3.20, the air volume

www.manaraa.com

flow rate discharged through each area element Q_i was determined using the continuity equation as follows

$$Q_i = V_{ref} \cdot A\left(V'_{i+1} - V'_i\right) \tag{4.2}$$

Ideal dispersion through each area element would be obtained in the limit of unvarying air flow along the duct axis, such that

$$Q_{ideal} = \frac{Q}{N} \tag{4.3}$$

Therein a useful definition of the deviation from uniform air dispersion is given by

$$\%\text{Deviation} = \sqrt{\frac{\sum[(Q_i - Q_{ideal})^2]}{N}} \times 10 \tag{4.4}$$

Based on this definition it is apparent that uniform air dispersion in a fabric air dispersion system would be indicated by a %Deviation value of zero.

The results of the air dispersion uniformity analysis are presented in Figures 4.15 though 4.21. The resulting %Deviation values for each case as calculated using Equation 4.4 are summarized in Table 4.4. This study demonstrated that the presence of the skeleton, along with its concomitant pressure loss, improved the uniformity of dispersion, relative to the case of no skeleton. Over a wide range of inlet flow rates (herein expressed in terms of the inlet Reynolds number), the no-skeleton cases exhibited a maximum deviation of 8.3% from ideal dispersion. The largest deviation for the corresponding skeleton cases was 6.1%. Therein when an adjustable flow device was situated at the mid-point of the duct and a skeleton was simultaneously present, the greatest deviation from ideal dispersion was 3.1%, over the range of inlet Reynolds numbers considered in the study.

www.manaraa.com

Table 4.1. Measured Static Pressure as a Function of Axial Location and Inlet Reynolds Number for Fabric Air Dispersion System with No Skeleton.

x	Re						
	125,000	157,000	190,000	224,000	255,000	287,000	320,000
	p						
m (ft)	Pa (in. wg)	Pa (in. wg)	Pa (in. wg)	Pa (in. wg)	Pa (in. wg)	Pa (in. wg)	Pa (in. wg)
0 (0)	32.4 (0.13)	47.3 (0.19)	72.2 (0.29)	92.1 (0.37)	119.5 (0.48)	141.9 (0.57)	166.8 (0.67)
2.44 (8)	34.9 (0.14)	54.8 (0.22)	77.2 (0.31)	102.1 (0.41)	132.0 (0.53)	164.3 (0.66)	199.2 (0.80)
4.88 (16)	47.3 (0.19)	67.2 (0.27)	89.6 (0.36)	119.5 (0.48)	151.9 (0.61)	186.8 (0.75)	226.6 (0.91)
7.32 (24)	47.3 (0.19)	69.7 (0.28)	97.1 (0.39)	134.5 (0.54)	166.8 (0.67)	206.7 (0.83)	249.0 (1.00)
9.75 (32)	57.3 (0.23)	84.7 (0.34)	114.5 (0.46)	151.9 (0.61)	189.2 (0.76)	231.6 (0.93)	276.4 (1.11)
12.19 (40)	47.3 (0.19)	72.2 (0.29)	102.1 (0.41)	137.0 (0.55)	176.8 (0.71)	221.6 (0.89)	271.4 (1.09)

www.manaraa.com

Table 4.2. Measured Static Pressure as a Function of Axial Location and Inlet Reynolds Number for Fabric Air Dispersion System with Skeleton.

x	Re						
	123,000	155,000	187,000	219,000	252,000	283,000	316,000
	p						
m (ft)	Pa (in. wg)	Pa (in. wg)	Pa (in. wg)	Pa (in. wg)	Pa (in. wg)	Pa (in. wg)	Pa (in. wg)
0 (0)	32.4 (0.13)	54.8 (0.22)	77.2 (0.31)	104.6 (0.42)	132.0 (0.54)	164.3 (0.66)	196.7 (0.79)
2.44 (8)	34.9 (0.14)	54.8 (0.22)	77.2 (0.31)	102.1 (0.41)	132.0 (0.54)	164.3 (0.66)	199.2 (0.80)
4.88 (16)	34.9 (0.14)	57.3 (0.23)	79.7 (0.32)	104.6 (0.42)	134.5 (0.54)	169.3 (0.68)	206.7 (0.83)
7.32 (24)	39.8 (0.16)	62.3 (0.25)	89.6 (0.36)	122.0 (0.49)	154.4 (0.62)	194.2 (0.78)	231.6 (0.93)
9.75 (32)	44.8 (0.18)	67.2 (0.27)	94.6 (0.38)	127.0 (0.51)	164.3 (0.66)	204.2 (0.82)	249.0 (1.00)
12.19 (40)	47.3 (0.19)	74.7 (0.30)	102.1 (0.41)	132.0 (0.53)	174.3 (0.70)	214.1 (0.86)	261.5 (1.05)

www.manaraa.com

Table 4.3. Calculated T’(0) Values for Fabric Air Dispersion System.

Skeleton Absent		Skeleton Present	
Inlet Re	T'(0)	Inlet Re	T'(0)
125,000	2.60	123,000	2.76
157,000	2.52	155,000	2.67
190,000	2.44	187,000	2.60
224,000	2.36	219,000	2.53
255,000	2.31	252,000	2.47
287,000	2.25	283,000	2.41
320,000	2.19	316,000	2.35

www.manaraa.com

Table 4.4. Calculated %Deviation Values.

Re	135,000	162,000	188,000	215,000	242,000	269,000	296,000
Average Q' L/s (CFM/ft^2)	5.90 (12.5)	7.08 (15.0)	8.26 (17.5)	9.44 (20.0)	10.62 (22.5)	11.80 (25.0)	12.98 (27.5)
%Deviation (no skeleton)	6.18%	6.56%	6.92%	7.27%	7.62%	7.96%	8.29%
%Deviation (skeleton)	4.68%	4.93%	5.17%	5.40%	5.64%	5.87%	6.09%
%Deviation (adjustable flow device)	2.56%	2.65%	2.76%	2.85%	2.93%	3.02%	3.11%

www.manaraa.com

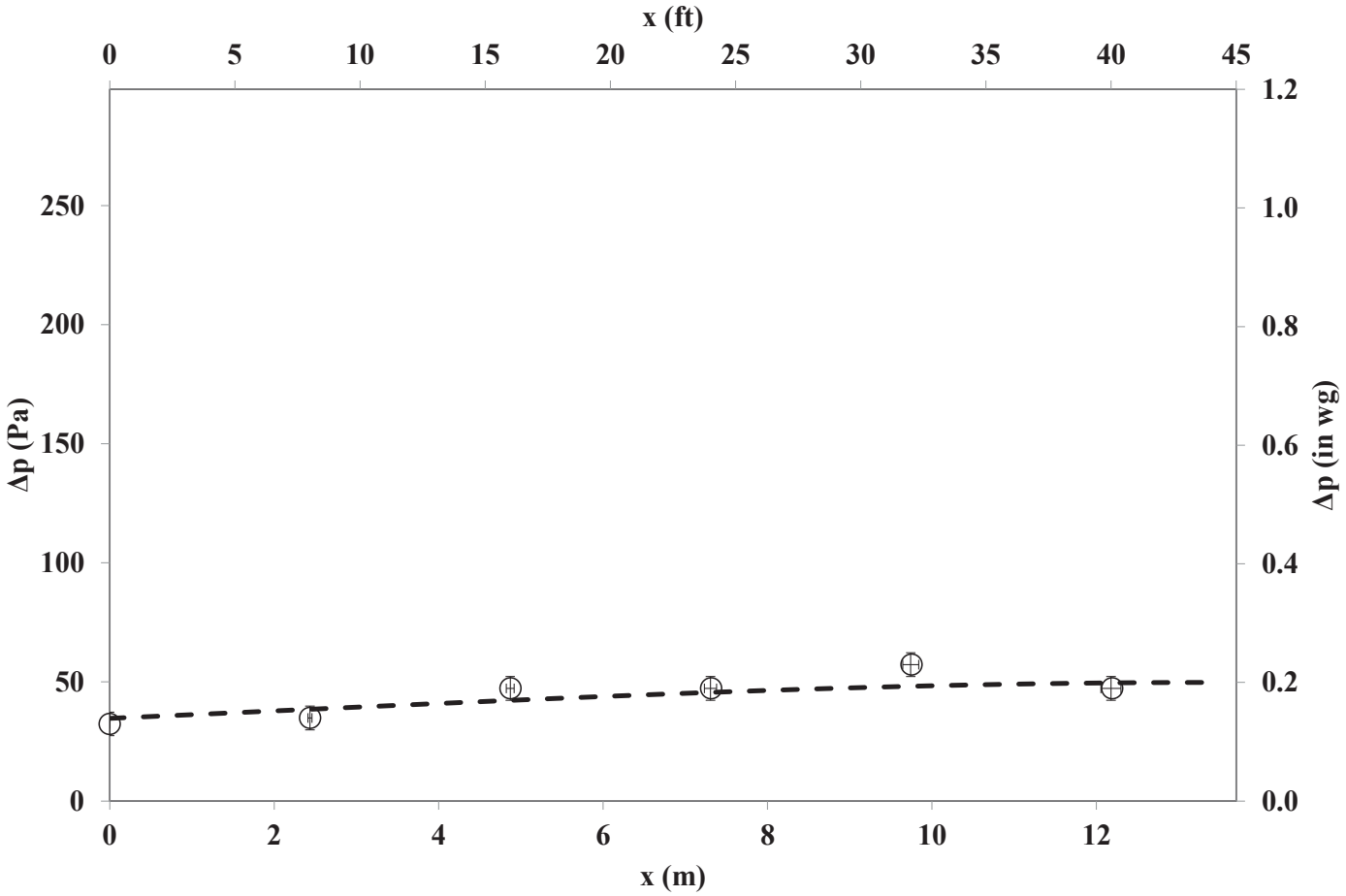

Figure 4.1. Comparison Between Experimental Data and Model for Re = 125,000 and No Skeleton.

www.manaraa.com

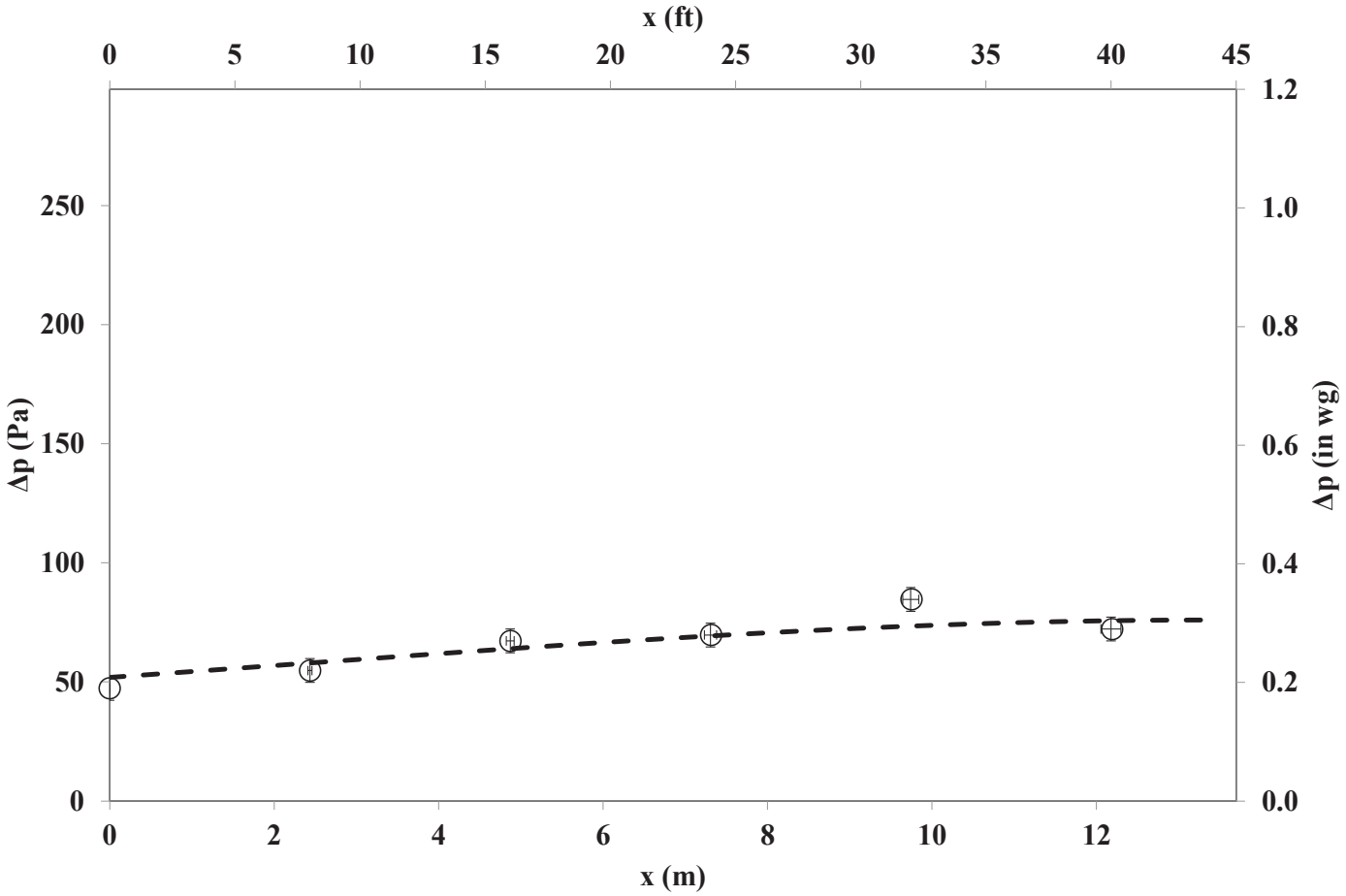

Figure 4.2. Comparison Between Experimental Data and Model for Re = 157,000 and No Skeleton.

www.manaraa.com

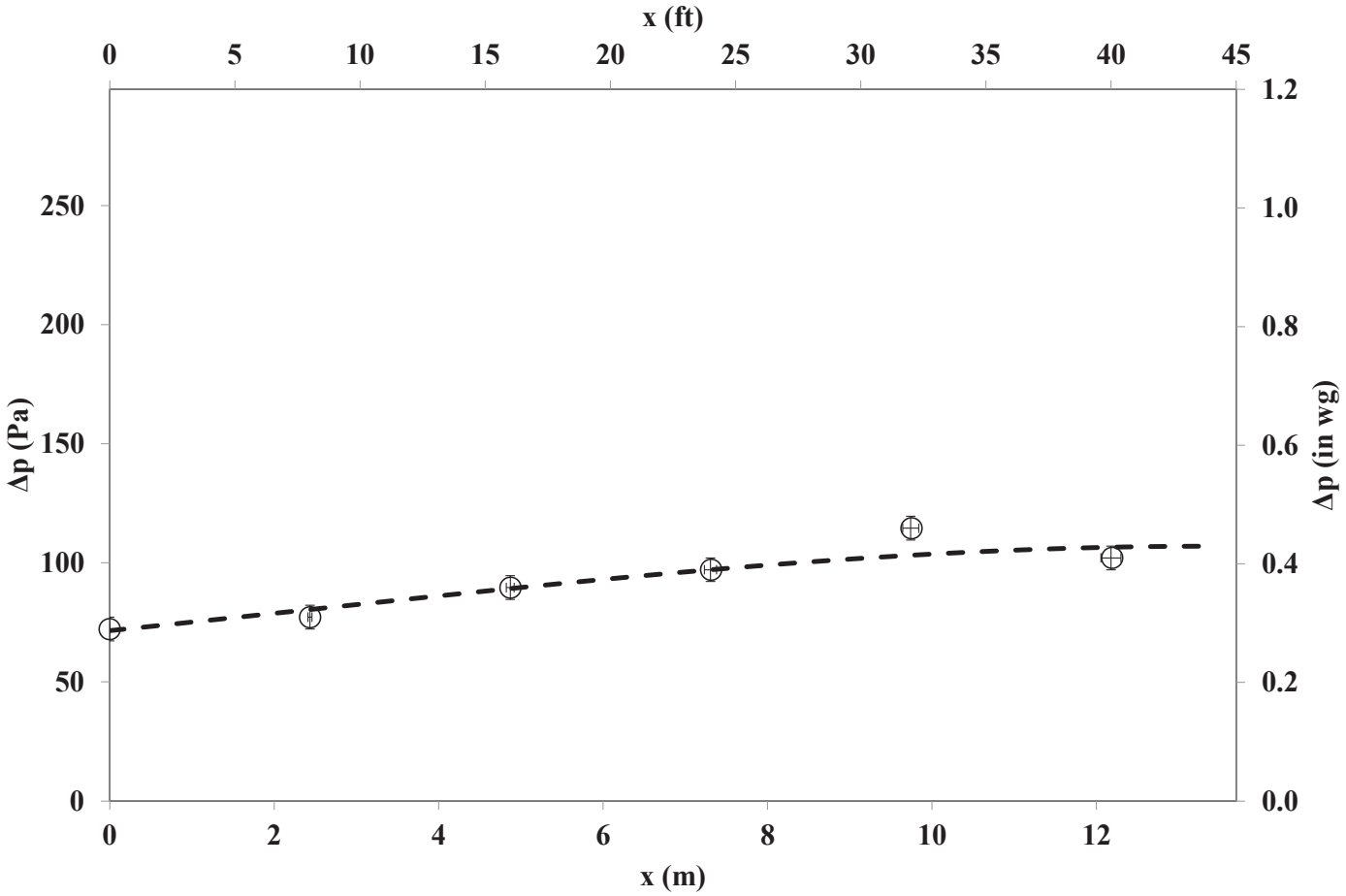

Figure 4.3. Comparison Between Experimental Data and Model for Re = 190,000 and No Skeleton.

www.manaraa.com

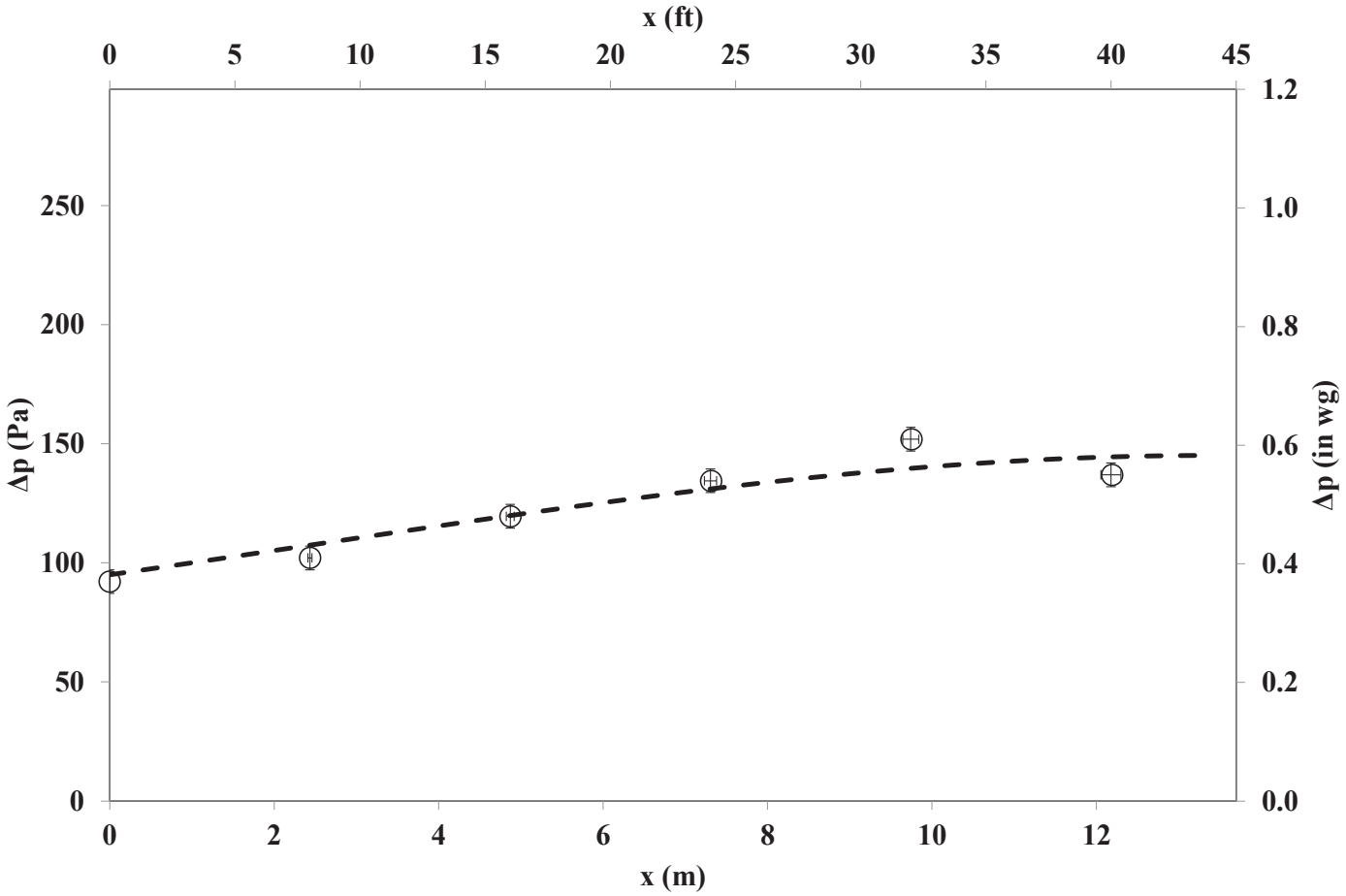

Figure 4.4. Comparison Between Experimental Data and Model for Re = 224,000 and No Skeleton.

www.manaraa.com

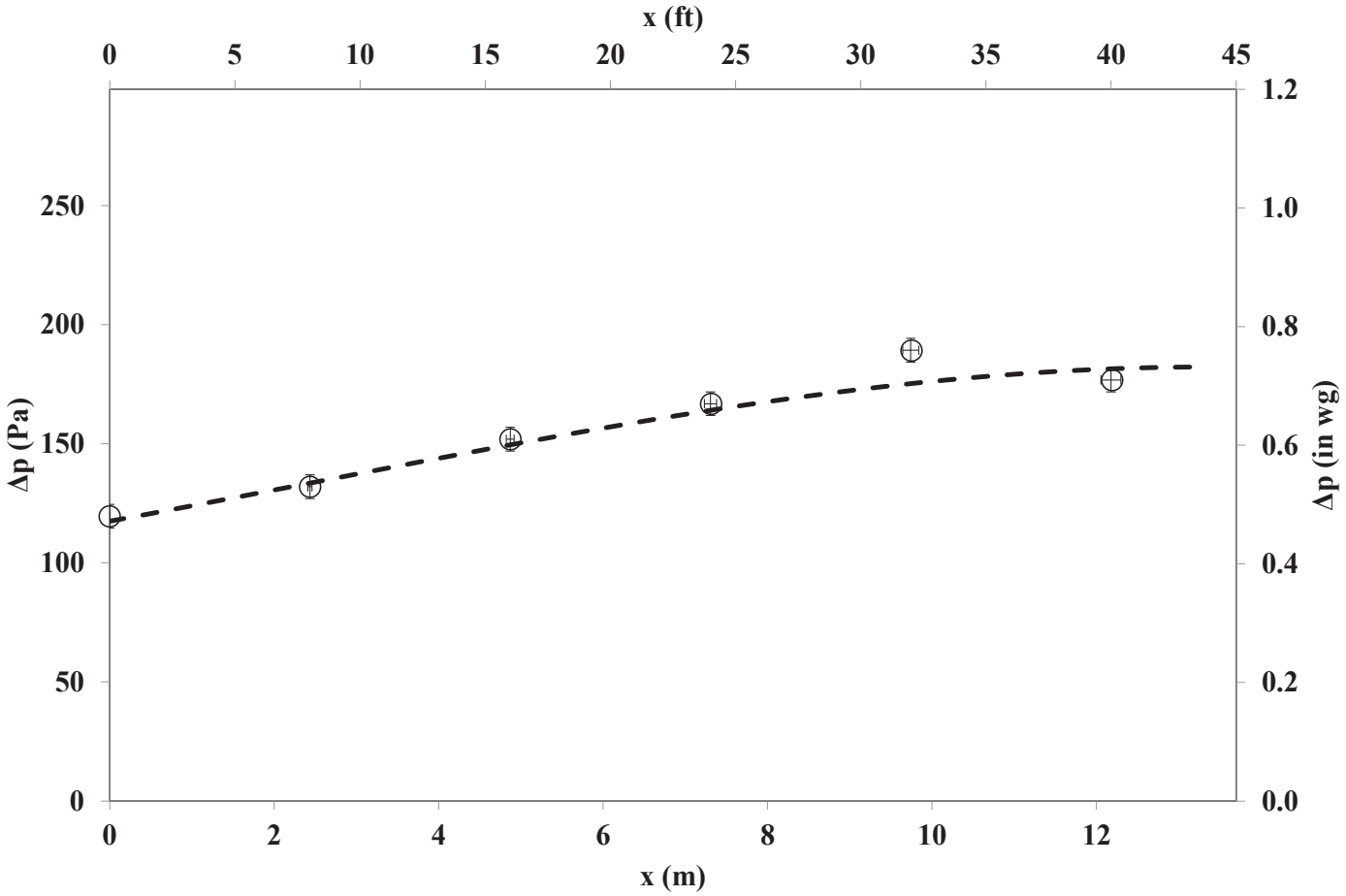

Figure 4.5. Comparison Between Experimental Data and Model for Re = 255,000 and No Skeleton.

www.manaraa.com

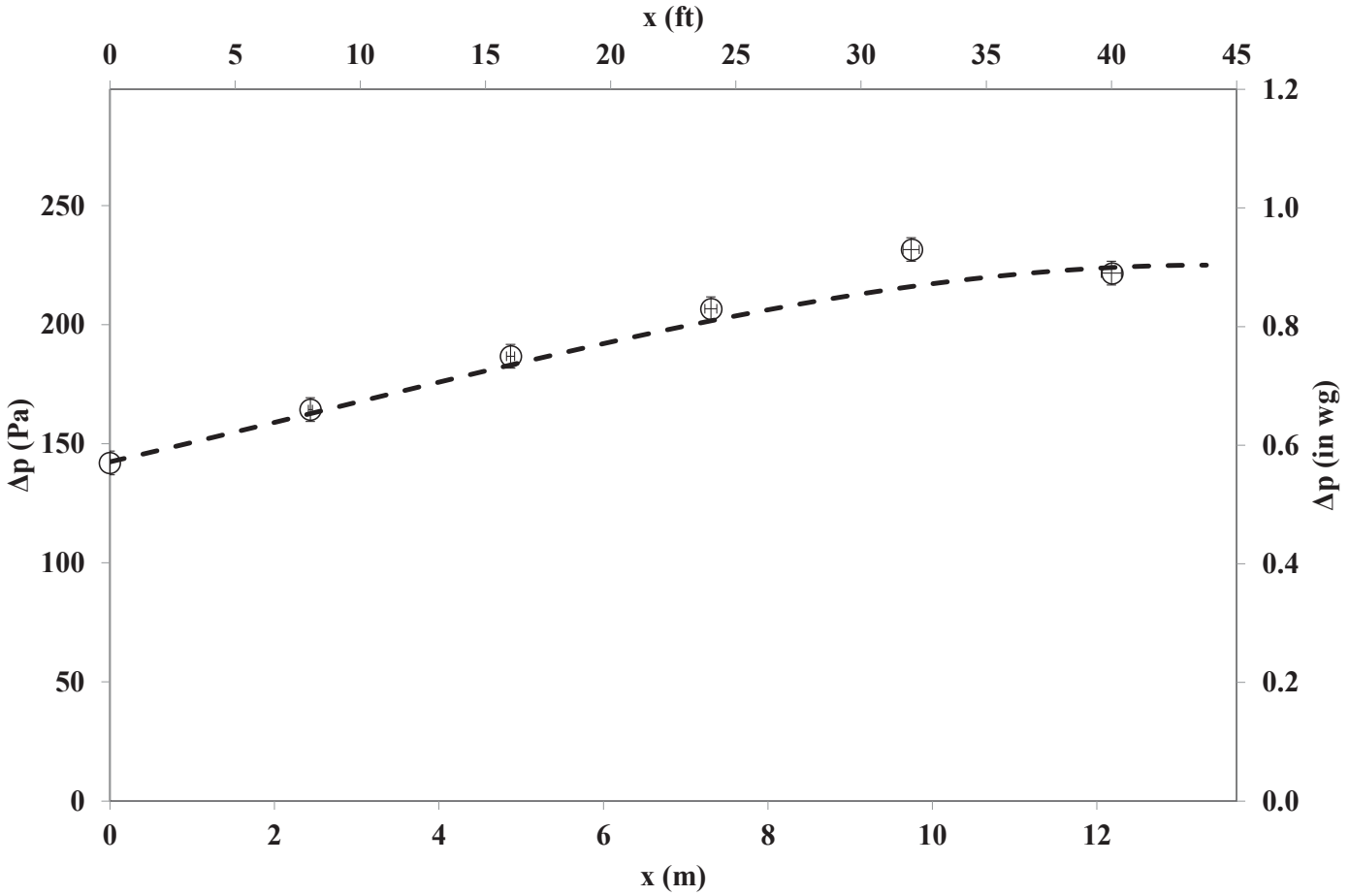

Figure 4.6. Comparison Between Experimental Data and Model for Re = 287,000 and No Skeleton.

www.manaraa.com

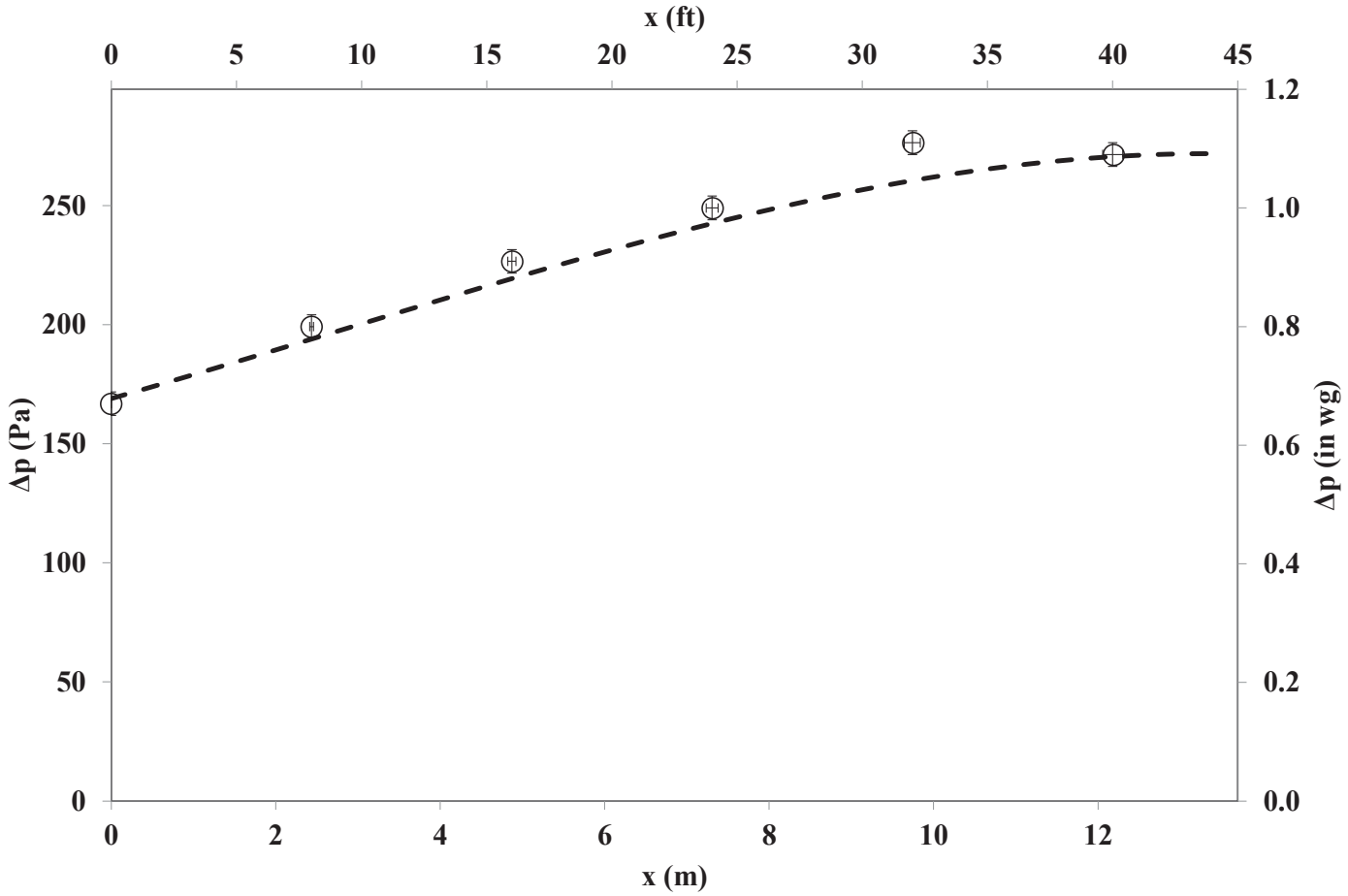

Figure 4.7. Comparison Between Experimental Data and Model for Re = 320,000 and No Skeleton.

www.manaraa.com

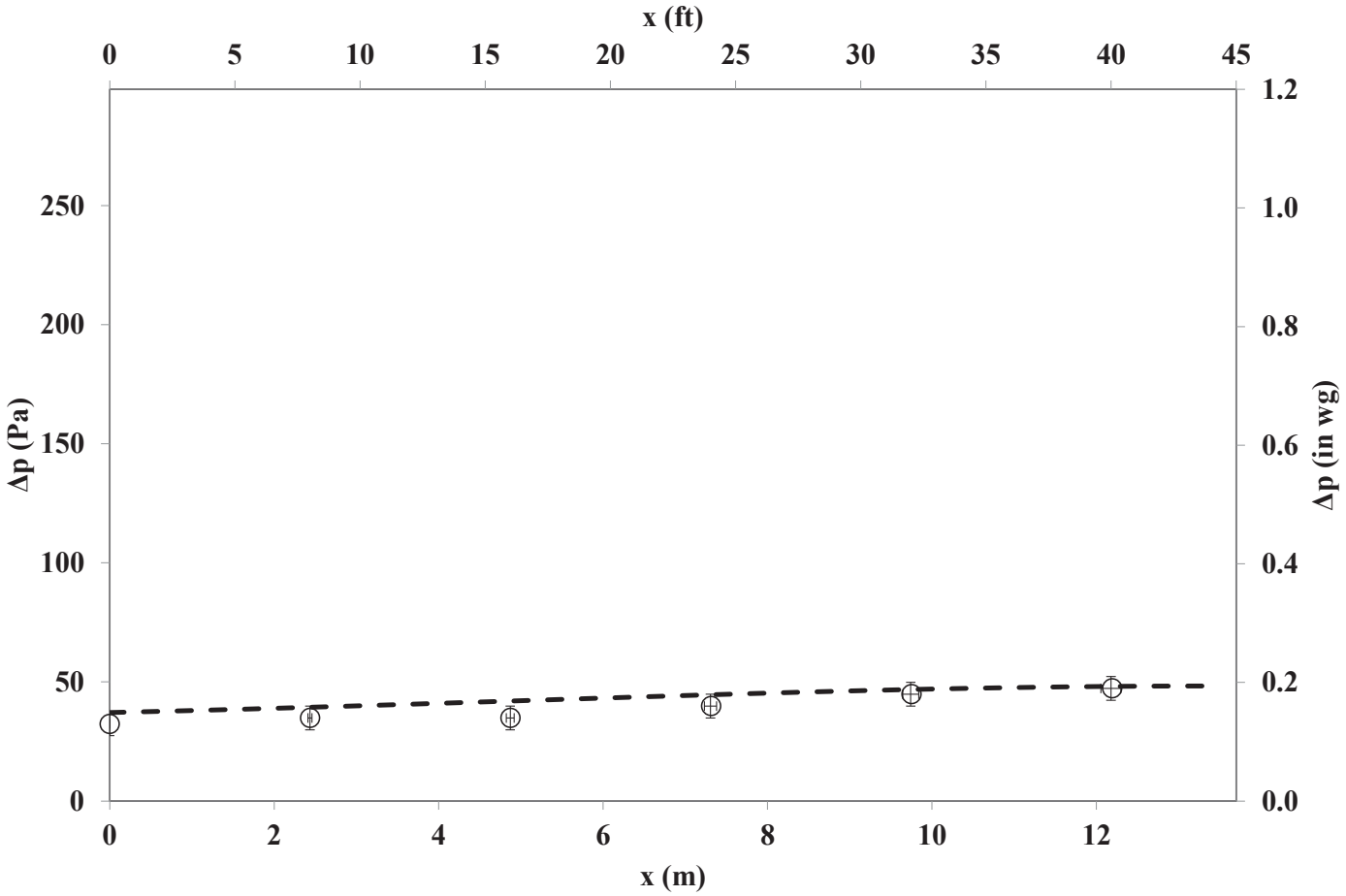

Figure 4.8. Comparison Between Experimental Data and Model for Re = 123,000 and an Internal Skeleton.

www.manaraa.com

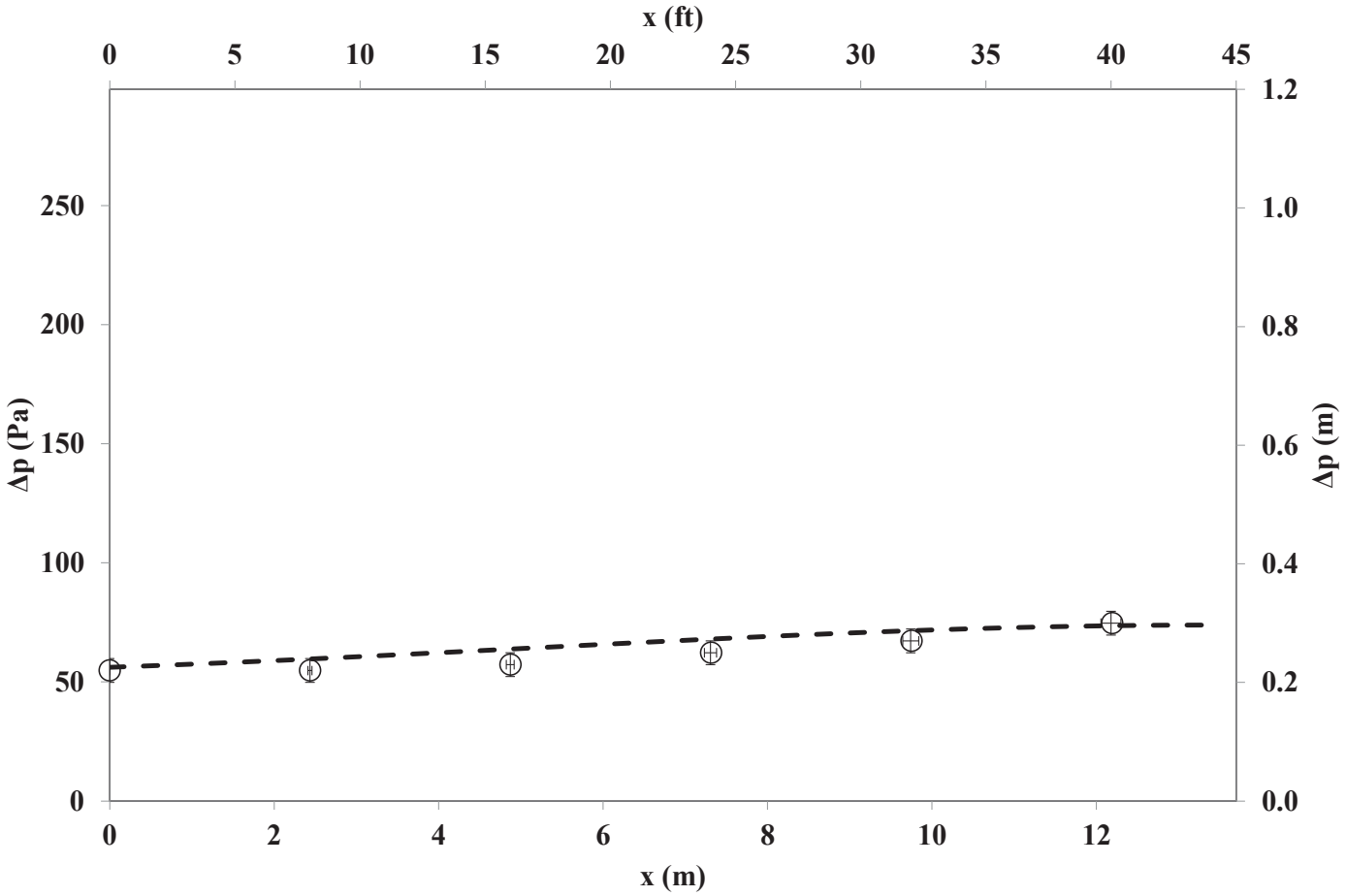

Figure 4.9. Comparison Between Experimental Data and Model for Re = 155,000 and an Internal Skeleton.

www.manaraa.com

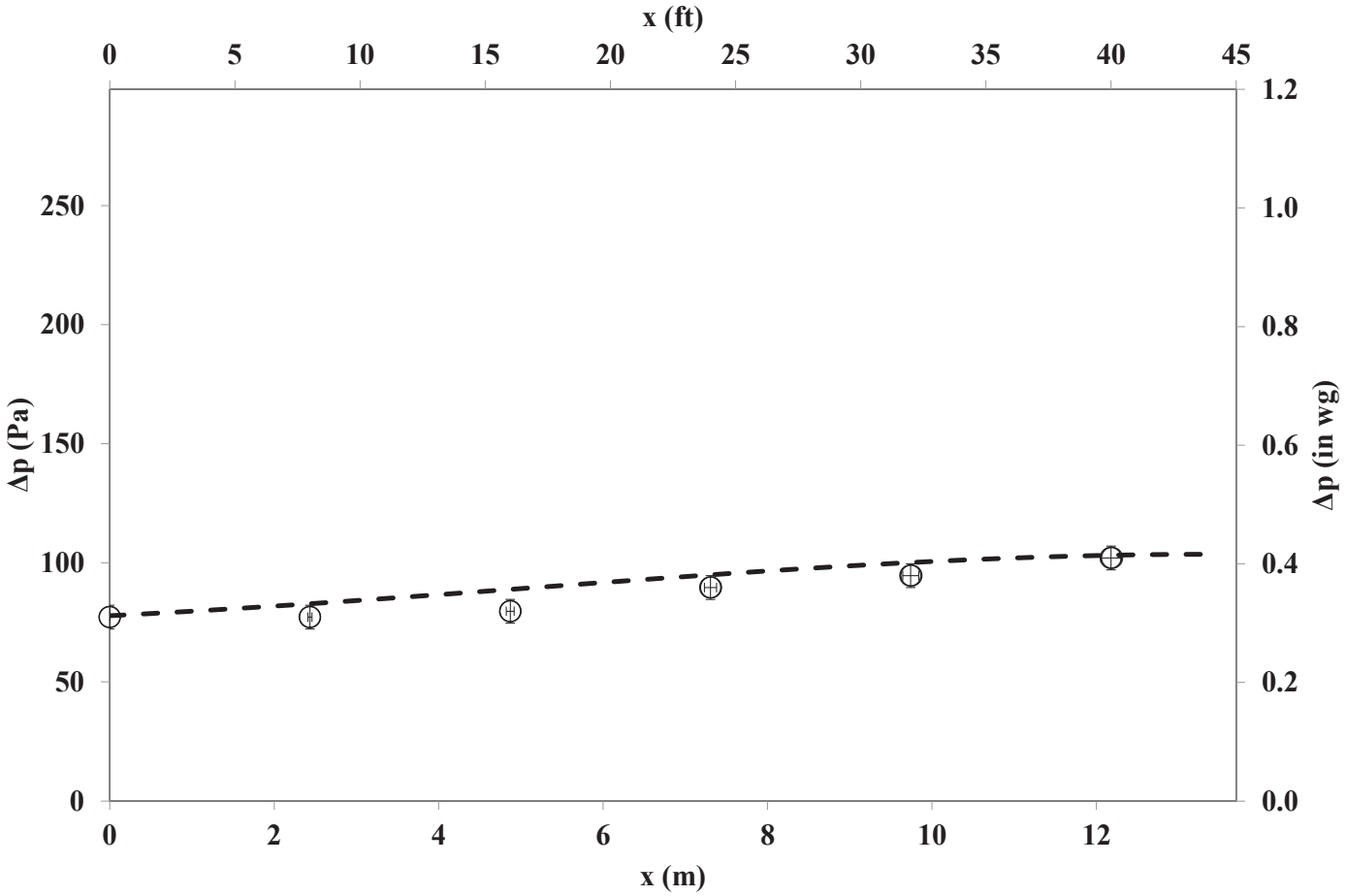

Figure 4.10. Comparison Between Experimental Data and Model for Re = 187,000 and an Internal Skeleton.

www.manaraa.com

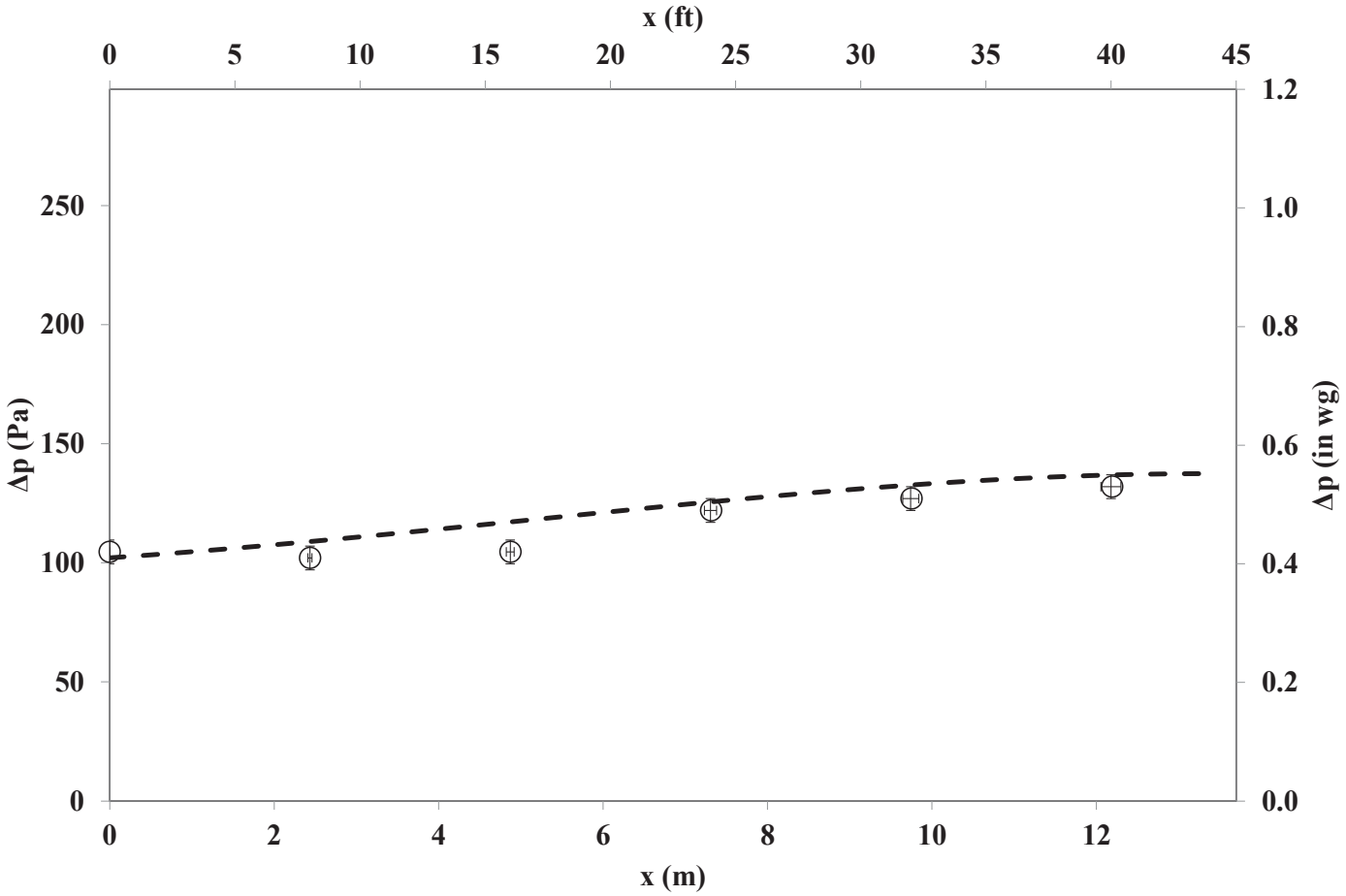

Figure 4.11. Comparison Between Experimental Data and Model for Re = 219,000 and an Internal Skeleton.

www.manaraa.com

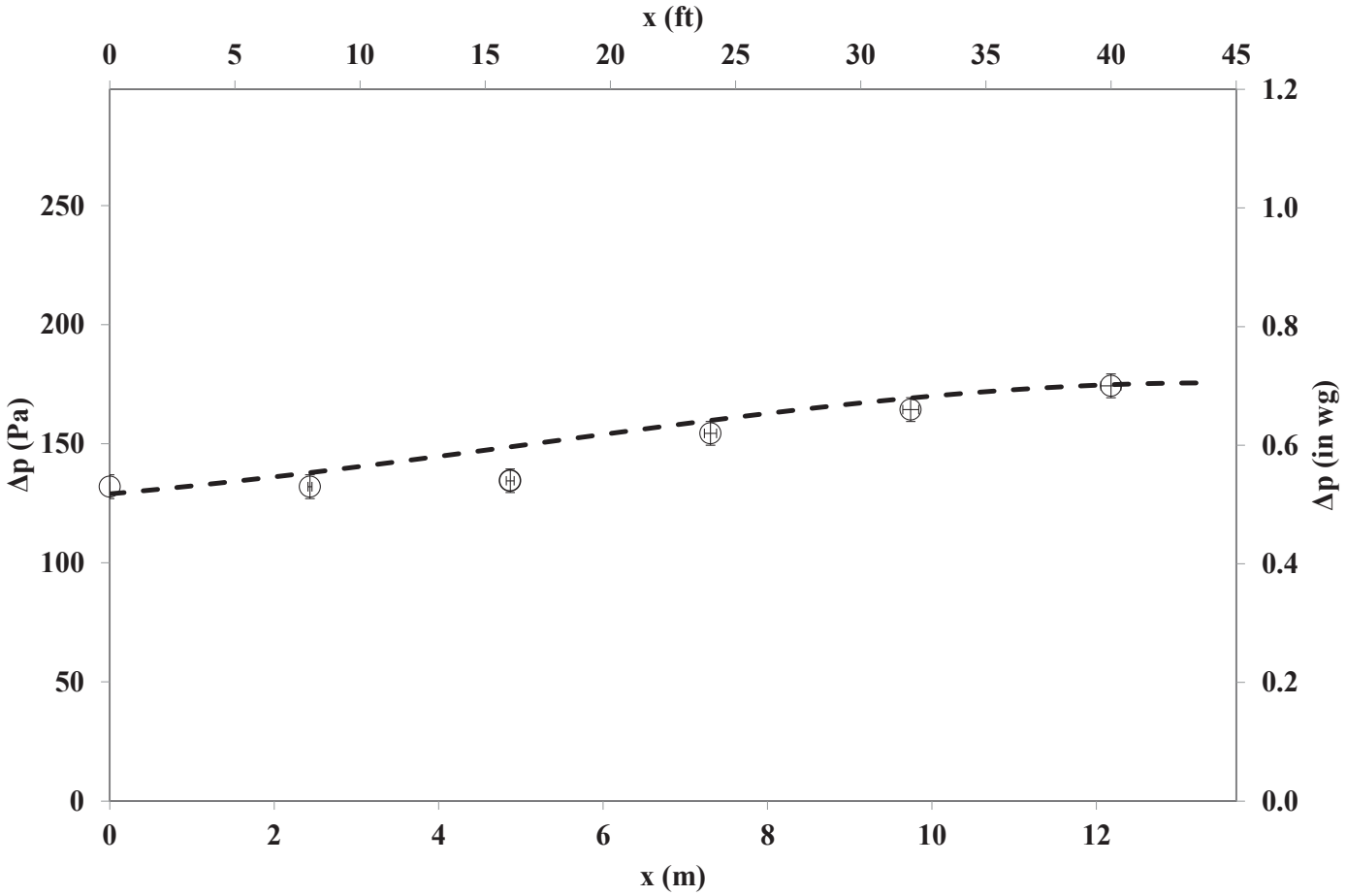

Figure 4.12. Comparison Between Experimental Data and Model for Re = 252,000 and an Internal Skeleton.

www.manaraa.com

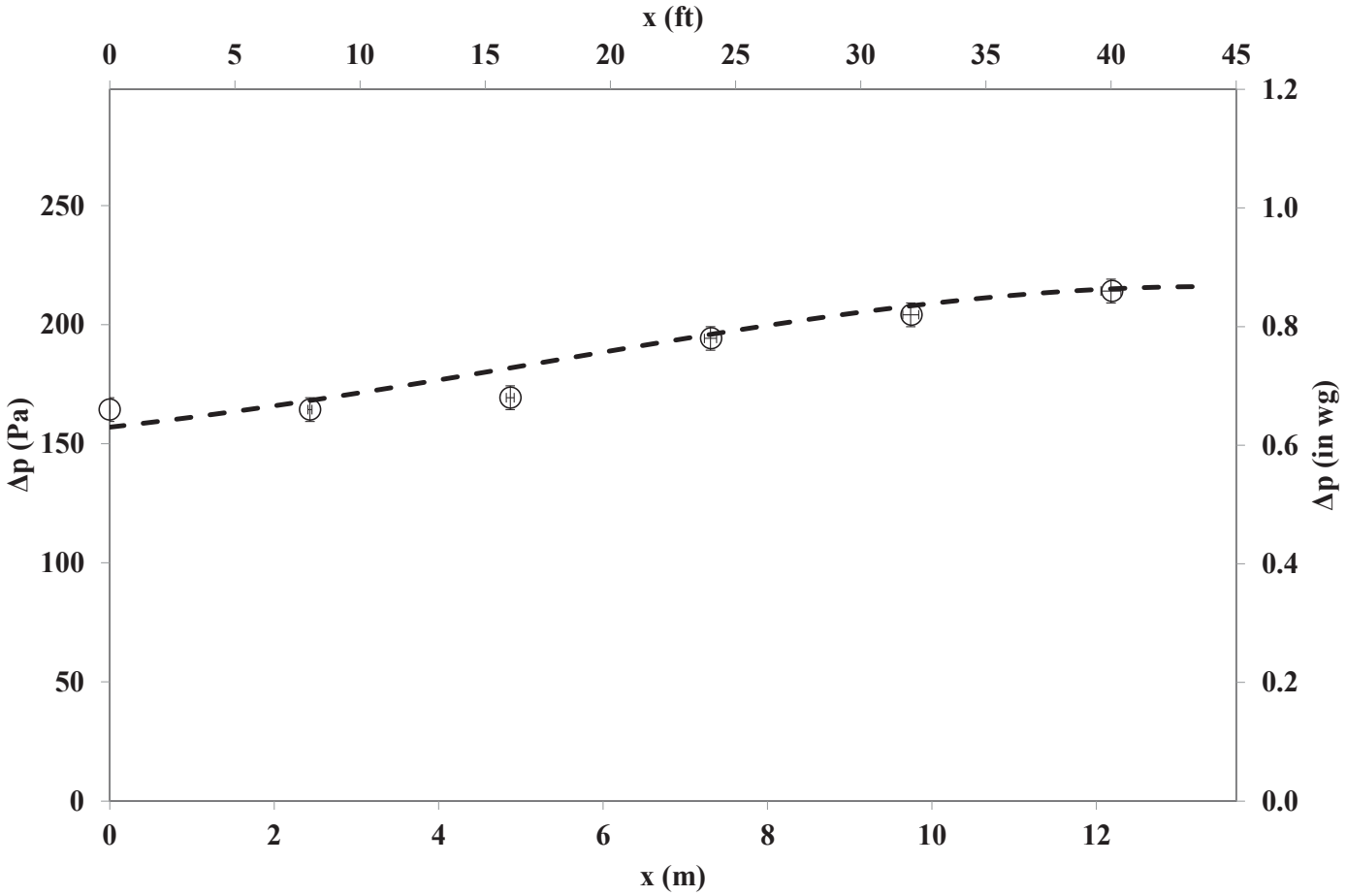

Figure 4.13. Comparison Between Experimental Data and Model for Re = 283,000 and an Internal Skeleton.

www.manaraa.com

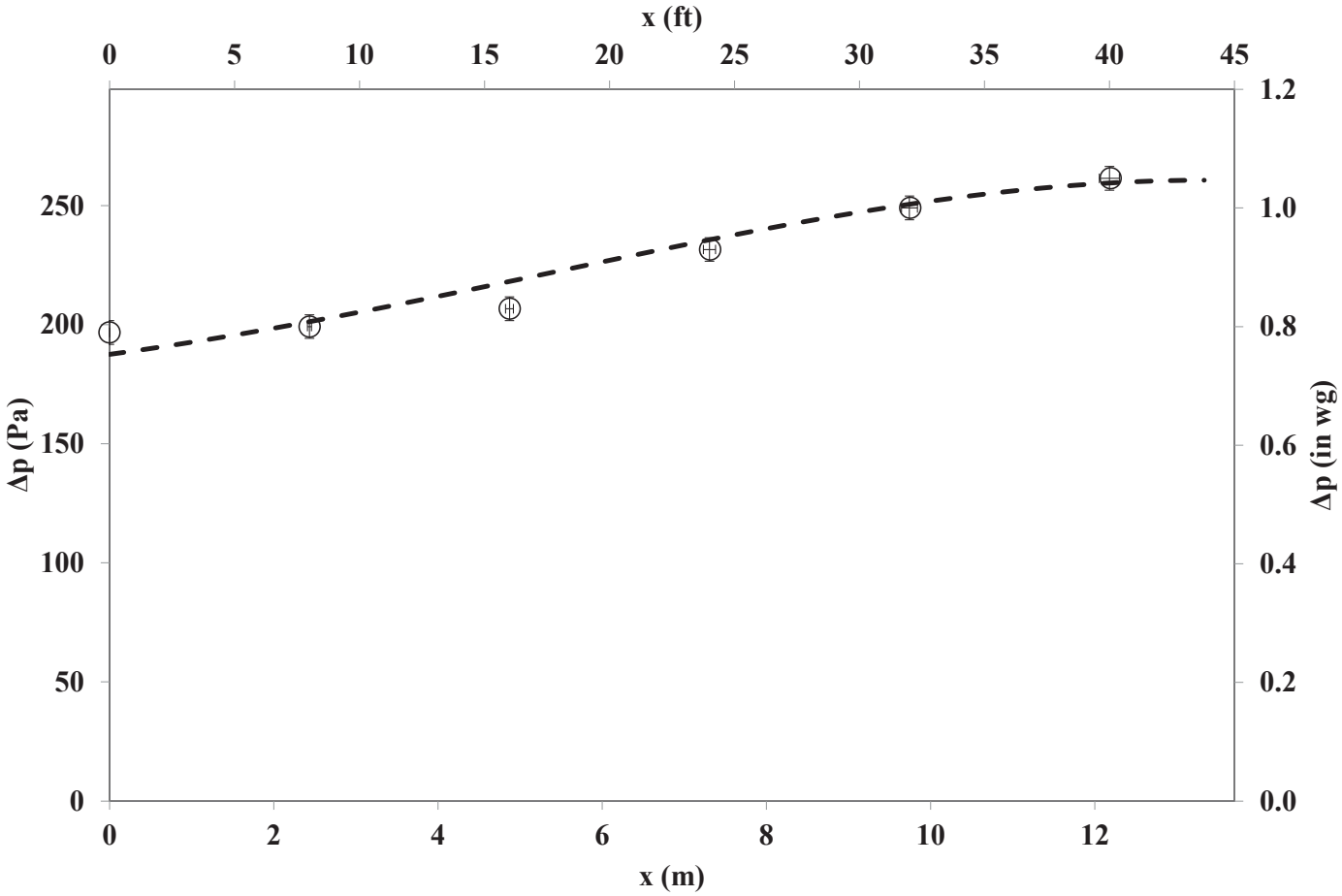

Figure 4.14. Comparison Between Experimental Data and Model for Re = 316,000 and an Internal Skeleton.

www.manaraa.com

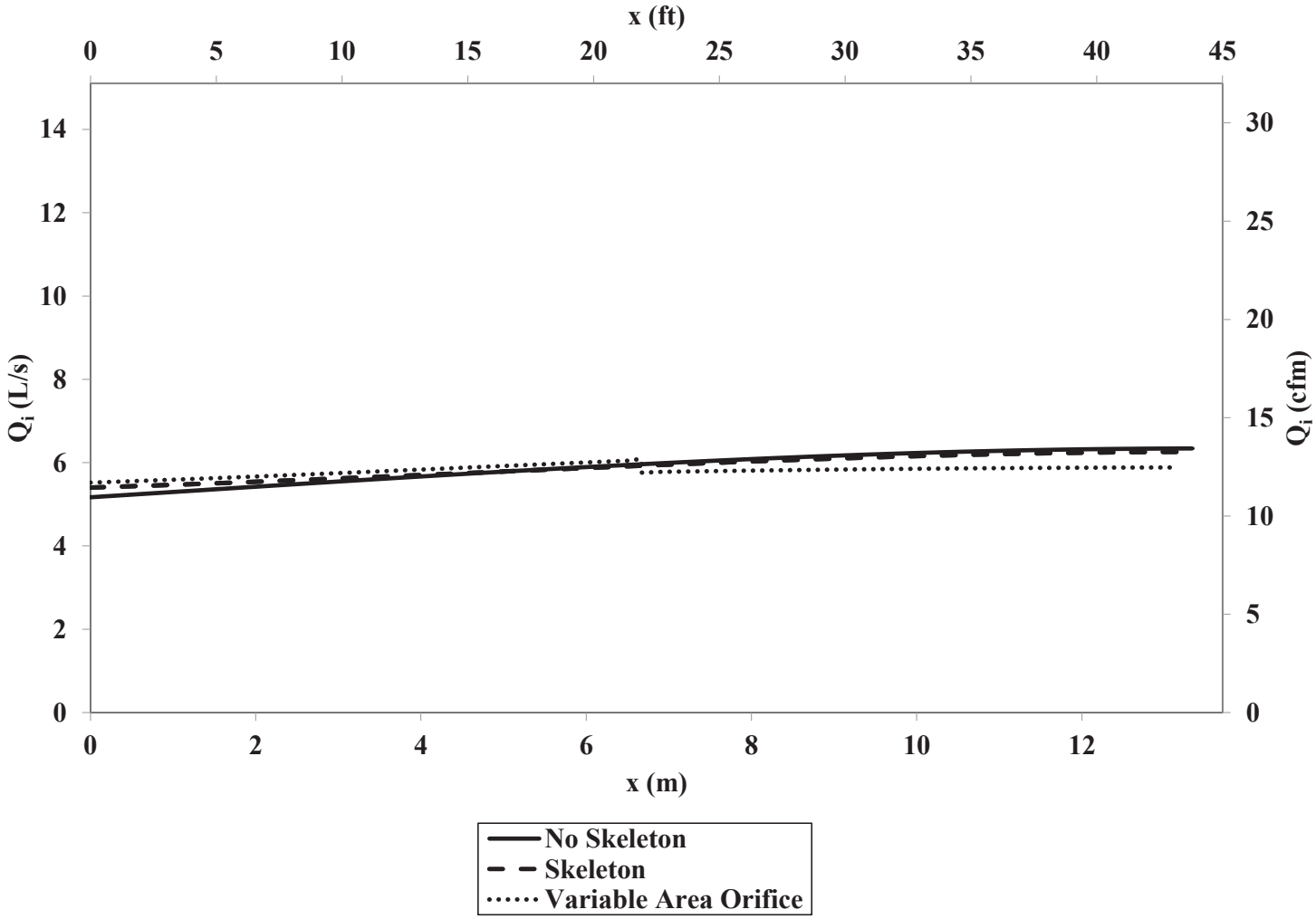

Figure 4.15. Comparison Between Q_i Distribution for No Skeleton, Skeleton, and Variable Area Cases at Re = 135,000.

www.manaraa.com

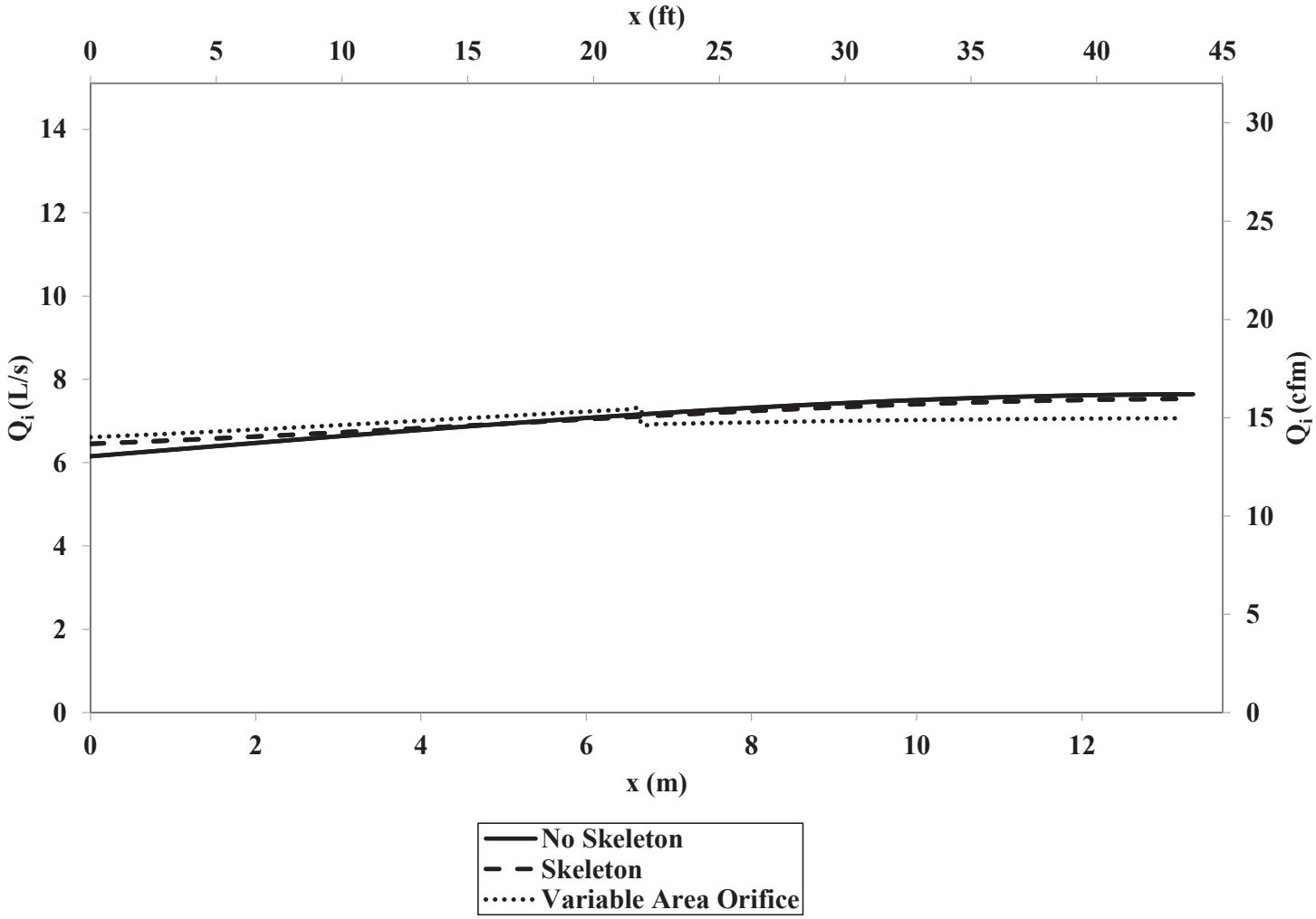

Figure 4.16. Comparison Between Q_i Distribution for No Skeleton, Skeleton, and Variable Area Cases at Re = 162,000.

www.manaraa.com

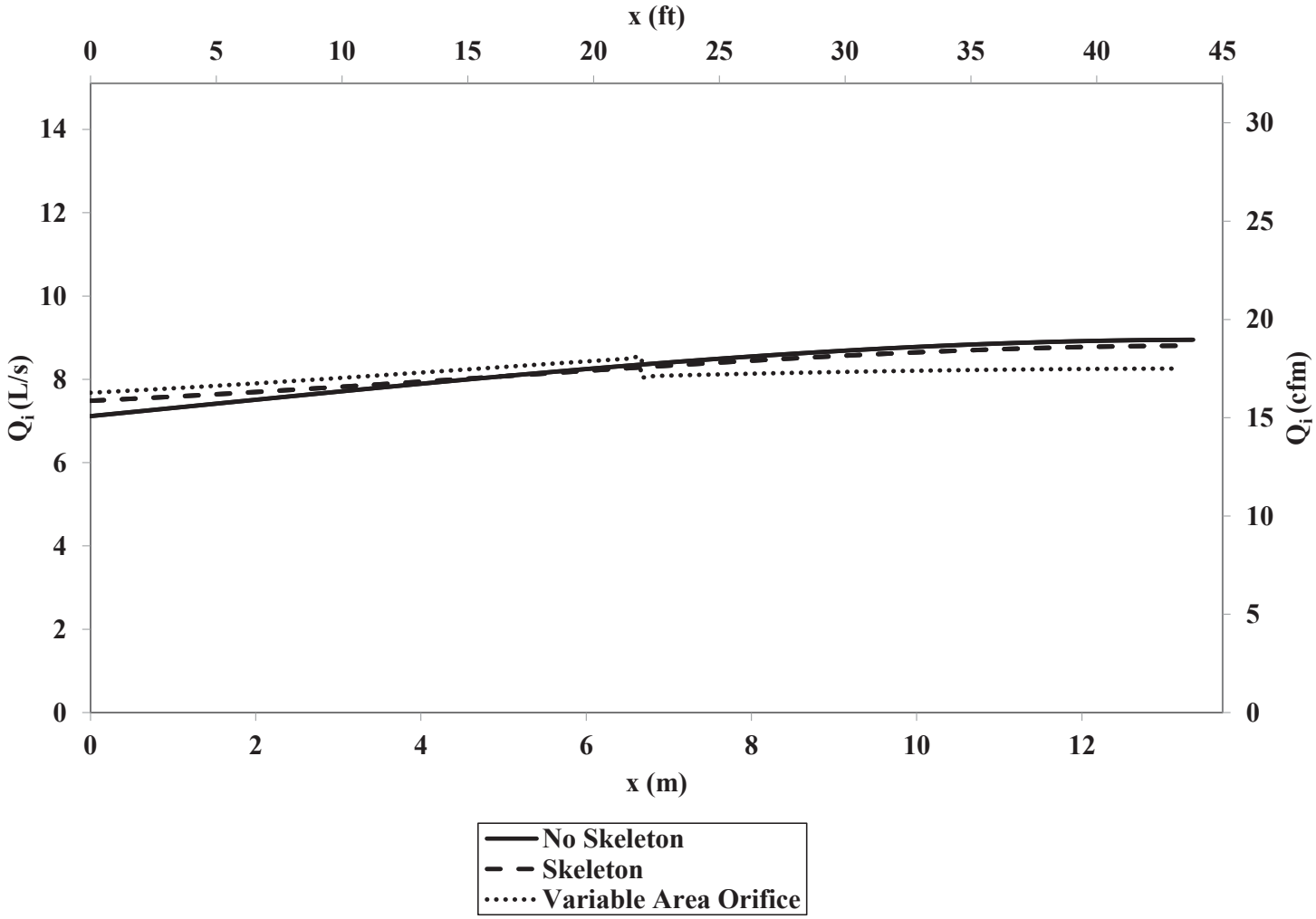

Figure 4.17. Comparison Between Q_i Distribution for No Skeleton, Skeleton, and Variable Area Orifice at Re = 188,000.

www.manaraa.com

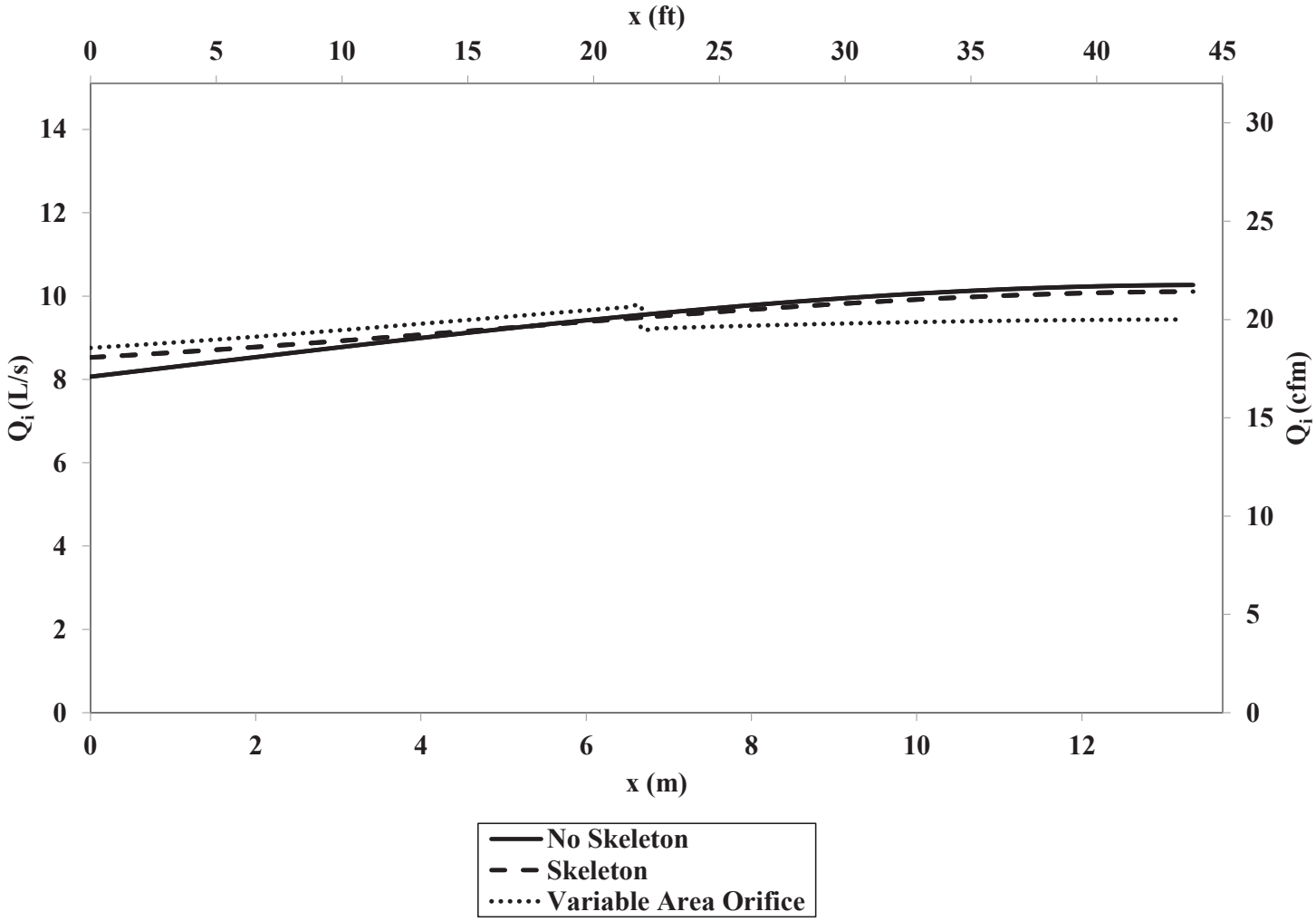

Figure 4.18. Comparison Between Q_i Distribution for No Skeleton, Skeleton, and Variable Area Orifice at Re = 215,000.

www.manaraa.com

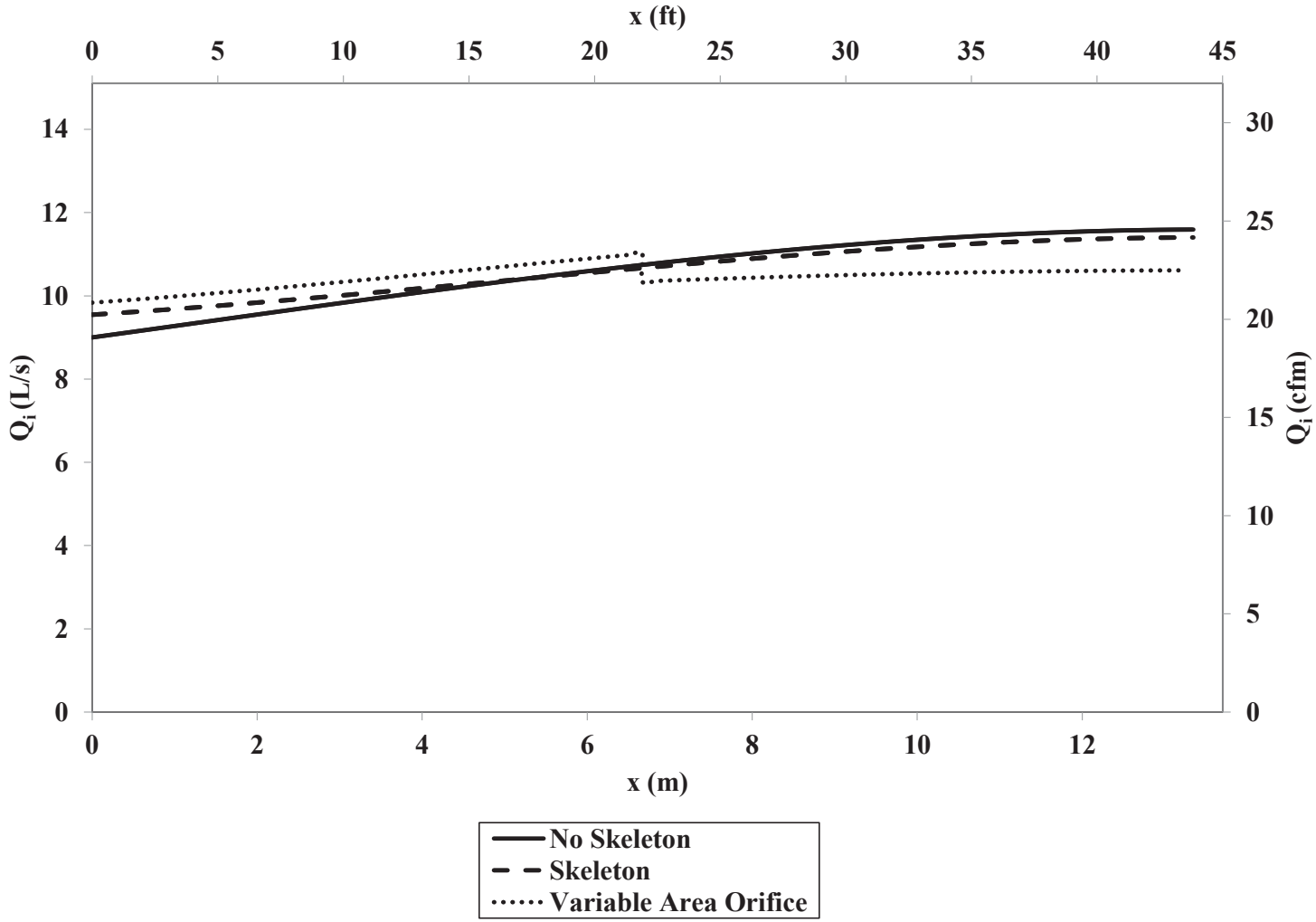

Figure 4.19. Comparison Between Q_i Distribution for No Skeleton, Skeleton, and Variable Area Orifice at Re = 242,000.

www.manaraa.com

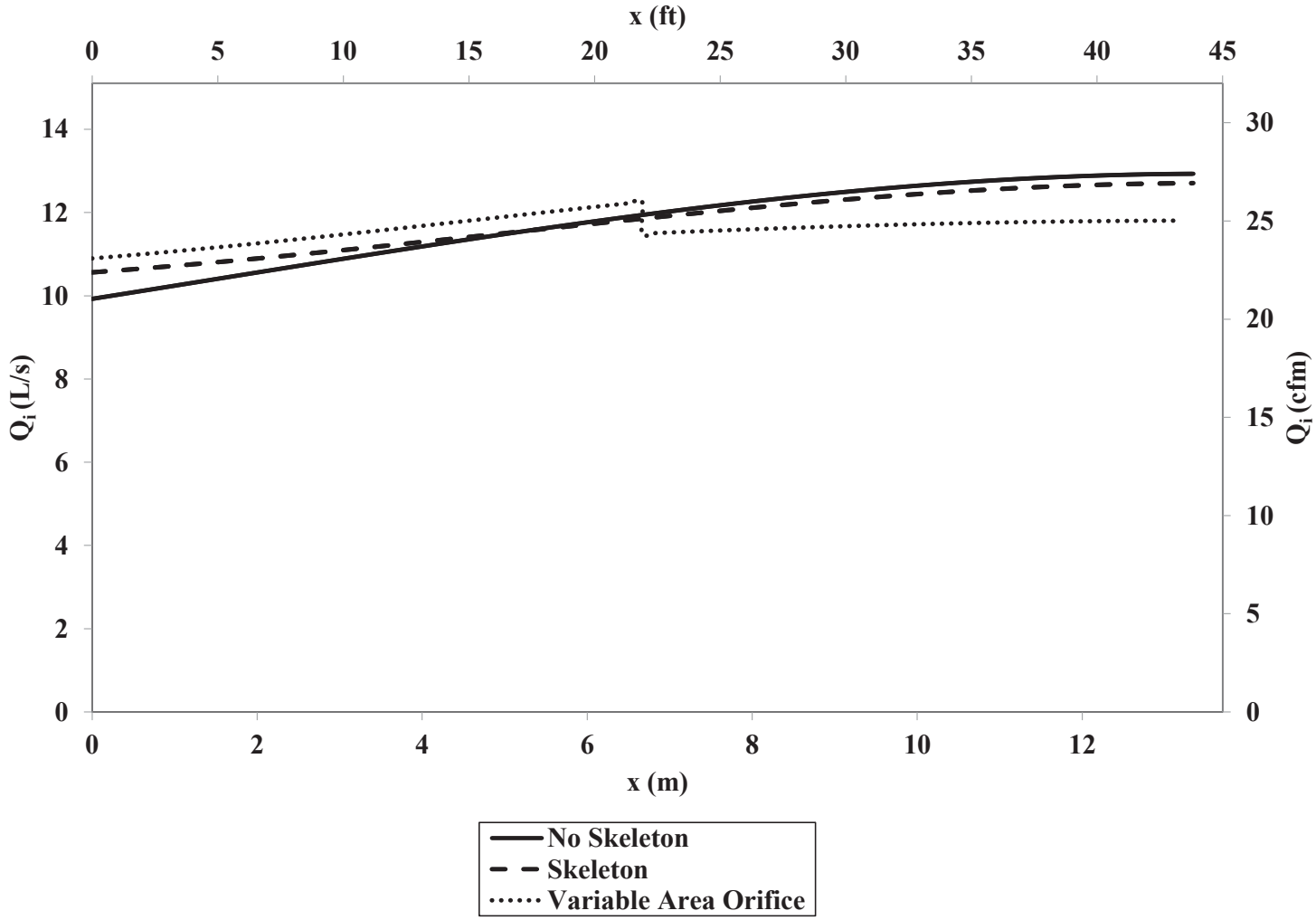

Figure 4.20. Comparison Between Q_i Distribution for No Skeleton, Skeleton, and Variable Area Orifice at Re = 269,000.

www.manaraa.com

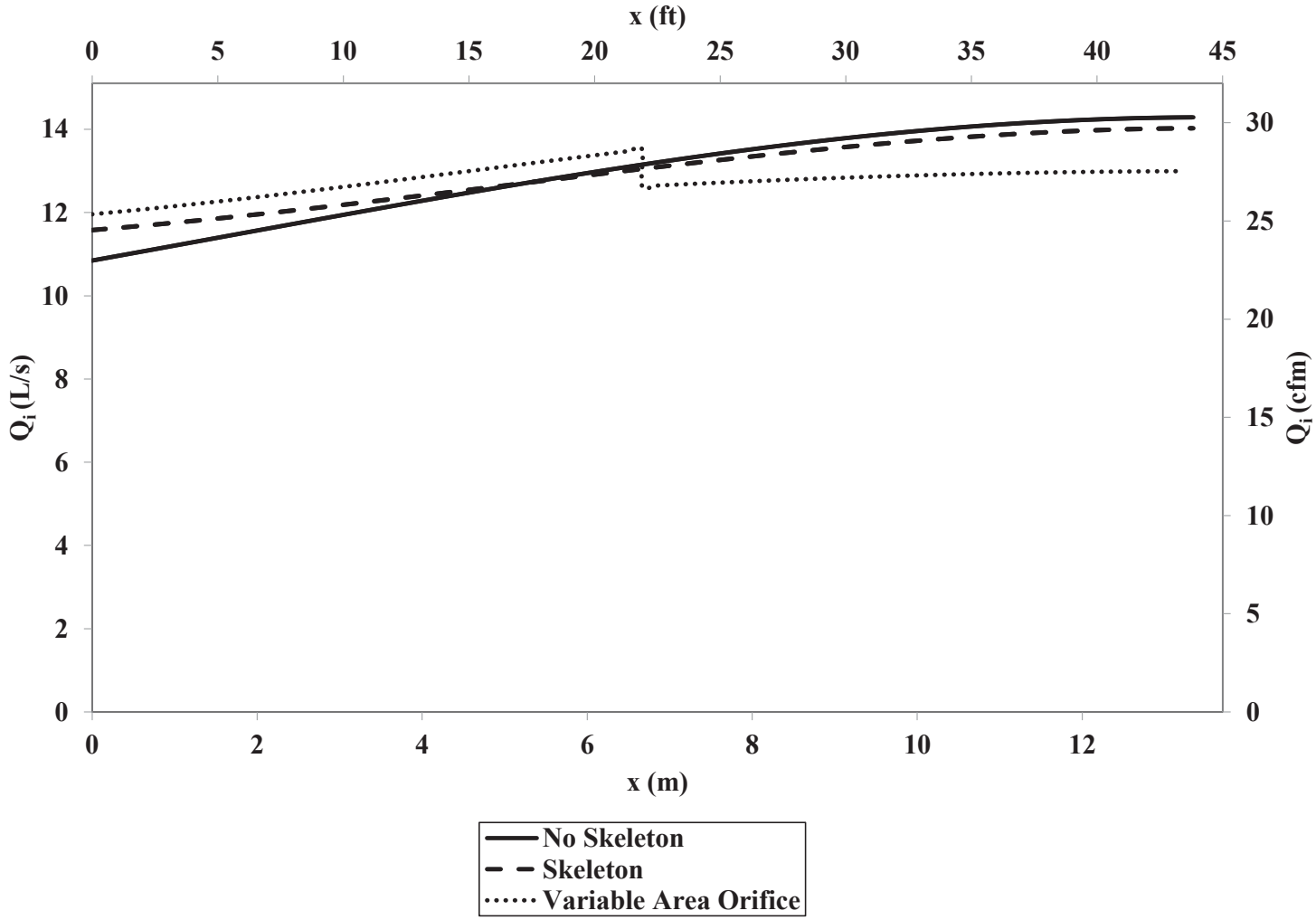

Figure 4.21. Comparison Between Q_i Distribution for No Skeleton, Skeleton, and Variable Area Orifice at Re = 296,000.

www.manaraa.com

CHAPTER 5

CONCLUSIONS

In this thesis a numerical model of fabric air dispersion system performance was developed. The investigation considered a round porous fabric duct having two rows of circular orifices arrayed in a triangular grid pattern along the lateral surfaces of the duct, when an internal skeleton was either present or absent. The differential equations governing the performance of the air dispersion system were derived by performing mechanical energy and mass balances across a specified duct section, and assuming that local air dispersion was a combined function of flow through the open cross section of the orifices and diffusion through the woven textile material. The air flow through the fabric was modeled in terms of a constant diffusion coefficient. This quantity was evaluated based on measurements of air volume flow rate per unit fabric surface area when a prescribed pressure loss was maintained across the textile material; the fabric diffusion data were provided by the duct manufacturer. The air flow through each lateral orifice was calculated assuming a standard empirical approach, wherein the volume flow through each orifice was assumed to be proportional to the square root of the pressure difference maintained across the open area of an orifice. The resulting two coupled first order ordinary differential air leakage equations were non-dimensionalized using the known total pressure and velocity at the entrance of the duct and the total duct length, and were solved using a straightforward numerical method. Such an approach has not been reported previously in the literature.

The model required certain input data, including such information as the ambient air density and pressure, the duct diameter and length, and the duct relative roughness. It

www.manaraa.com

was necessary to account for the presence or absence of the internal skeleton by adjusting the latter quantity. A notable feature of the model was that the input was expressed in terms of the ratio of the total orifice area to surface area, since this provided sufficient information related to the quantity and diameters of the lateral surface orifices. The numerical fabric air dispersion model was experimentally verified by comparing measured static pressures in the duct to those values predicted by the numerical model. Therein a constant representative value of orifice coefficient was deemed to yield accurate predictions of system performance. In general the model predicted the performance of the system quite well, even with a simplified assumption regarding the orifice loss coefficient. Predictions of the static pressure variation longitudinally through a duct system generally deviated by less than 3% from measured static pressure data. The numerical model should apply over a wide range of circular orifice diameters and patterns, and is potentially a useful design tool for such systems.

Ensuring consistent air flow along the duct axis is critical to the proper design of an air dispersion system. Hence once the numerical air dispersion model was experimentally verified, a further study was conducted to characterize the uniformity of air dispersion along the flow axis of a similar fabric air dispersion system. Therein the entering volume flow rate was systematically varied over a representative range. Several cases were considered, e.g., a skeleton was either absent or present in the duct. In addition, the study also investigated the situation where an adjustable flow device was installed at the mid-point of the duct where an internal skeleton was simultaneously present. Such an adjustable flow device is capable of imposing a specified pressure loss at a specific axial location in the duct. This study demonstrated that the presence of the skeleton improved the uniformity

www.manaraa.com

of dispersion relative to the case of no skeleton, albeit at the expense of a higher total pressure at the entrance to the duct. Enhanced air dispersion uniformity was likewise obtained by use of the adjustable fabric orifice. Manufacturers of fabric air dispersion systems recommend the use of such devices to balance static regain, control airflow to branches, reduce turbulence, and minimize abrupt start-ups.

It is suggested that further work be performed to further verify the model, and enhance its utility as a design tool. For example, it would be useful to verify whether the model can accurately predict performance of a similar air distribution system, i.e., one having identical orifice diameters and patterns and constructed from the same porous fabric, but having a different length or diameter. This is important because the variation of duct relative roughness with duct diameter has not been experimentally determined, particularly in association with the use of an internal skeleton. It would be desirable to establish whether the numerical model can be applied to air dispersion systems having a non-circular cross section. Likewise it is important to ascertain whether the model can readily be extended to fabric air dispersion systems having different circular orifice patterns or diameters. Additional testing should be conducted to quantify any variation of the orifice coefficient in the flow direction. Further experimental work should be completed to develop performance models for air dispersion systems that have linear slot orifices. It is important to confirm whether the model can accommodate fabric air dispersion systems that are intended for low face velocity applications where displacement ventilation is needed, i.e., the porous fabric alone is used to disperse the air and no orifices are present.

It is further recommended that pressure loss testing of fabric duct system fittings, e.g., elbows, transitions, divided flow tees or laterals, etc., be performed in order to have a

www.manaraa.com

well populated database of fittings, and therefore enhance the design of energy efficient fabric air dispersion systems. It is likewise proposed that experimental measurements (or CFD modeling) be used to evaluate the throw from the various orifice designs or the permeable fabric duct. It is likely that this quantity varies along the flow axis of the air dispersion system.

www.manaraa.com

REFERENCES

ASHRAE. 2005. ASHRAE Guideline 2-005, Engineering Analysis of Experimental Data. Atlanta: American Society of Heating, Refrigerating and Air-Conditioning Engineers, Inc.

ASHRAE. 2008. ANSI/ASHRAE Standard 120-2008, Method of Testing to Determine Flow Resistance of HVAC Ducts and Fittings. Atlanta: American Society of Heating, Refrigerating and Air-Conditioning Engineers, Inc.

Chen, Fujiang, Huanxin Chen, Junlong Xie, Zhaohui Shu, Chang Zhang, and Yunpeng Hu. 2010. Characterizing Airflow Through Fabric Air Dispersion System Using a Porous Media Model. *Energy and Buildings* 43: 665-70.

Chen, Fujiang, Huanxin Chen, Junlong Xie, Zhaohui Shu, and Jiani Mao. 2011. Air Distribution in Room Ventilated by Fabric Air Dispersion System. *Building and Environment* 46: 2121-129.

Haaland, S. E. 1983. Simple and Explicit Formulas for the Friction Factor in Turbulent Pipe Flow. *Journal of Fluids Engineering* 105: 89-90.

Kulkarni, D., A.N. Nalla, S. Idem, and K. Gebke. 2012. Laboratory Testing of a Fabric Air Dispersion System. *ASHRAE Transactions* 118(2):484-90.

Munson, Bruce Roy, T. H. Okiishi, and Wade W. Huebsch. 2009 *Fundamentals of Fluid Mechanics*. Hoboken, NJ: J. Wiley & Sons.

Nigam, Vandana, and Stephen Idem. 2003. A Duct Performance Model That Includes the Effects of Leakage. *ASHRAE Transactions* 109(1):431-38.

White, Frank M. 2006. *Viscous Fluid Flow*. New York, NY: McGraw-Hill.

www.manaraa.com

VITA

Mr. James Scott Leverette was born in Chattanooga, TN on March 13, 1990. He graduated from Boyd-Buchanan high school in 2008 as the class salutatorian. He entered college at Tennessee Technological University in the fall of 2008 and graduated magna cum laude with his Bachelor of Science in Mechanical Engineering in the spring of 2012. After this, he stayed on to work with the Industrial Assessment Center at TTU and obtained his Master of Science degree in Mechanical Engineering in 2013.

www.manaraa.com